# **Material Evaluation Using X-ray Computed Tomography**

Jennifer M. Sietins<sup>1</sup>, William H. Green<sup>1</sup>, Justin S. Jones<sup>2</sup>

- 1. DEVCOM Army Research Laboratory
- 2. NASA Goddard Space Flight Center

jennifer.m.sietins.civ@army.mil, william.h.green1.civ@army.mil, justin.s.jones@nasa.gov

Κe	ey points/objectives:	4
Gl	lossary	4
Αl	bstract	5
In	troduction	5
	1.1 XCT Fundamentals and Basic Parameters	7
	1.2 XCT History	9
	1.3 Materials Science Applications	11
	1.3.1 Comparisons with other NDE methods	12
	1.3.2 Complementary materials characterization techniques	14
2.	Advanced Scanning and Reconstruction Techniques	15
	2.1 Linear Detector Array	15
	2.2 Helical Scanning	17
	2.3 Dual Energy Scanning	18
	2.4 Phase Contrast	20
	2.5 Diffraction Contrast Tomography	21
	2.6 Open CT	22
	2.7 Static CT	23
	2.8 Cryogenic or Temperature Controlled CT	23
	2.9 In-situ Mechanical Testing	25
	Example 1: Compression loading of polymeric trusses	25
	Example 2: Tensile loading and cavity formation	26
	2.10 4D Scanning	27
	2.11 Iterative Reconstruction	27
3.	Post-scan Analyses	28
	3.1 Advanced segmentation	28
	3.2 Tolerance deviation analysis	30
	Example 1: Comparison of part deviations for different additive manufacturing methods	31
	Example 2: Quantification of deviations due to thermal residual stress	32
	Example 3: Deformation quantification of a helmet after impact testing	33
	3.3 Porosity Analysis	33
	Example 1: Reduction in porosity with improved processing	33
	Example 2: Understanding the relationship with mechanical performance	35

3.4 Fiber orientation	36
Example 1. Misaligned fibers between plies	36
Example 2. Additive manufacturing print orientation of chopped fiber filament	37
3.5 Failure Analysis	38
Example 1: Circuit board failure investigation	38
Example 2: Crack in AM Part	39
Example 3: Boroscope camera failure	40
Example 4: Astronaut Helmet Mishap Investigation	41
4. XCT Practical Limitations	42
4.1 Spatial resolution, field of view, and geometric unsharpness	42
4.1.1 Image quality indicators and representative quality indicators	45
4.2 Influences on X-ray attenuation	47
4.3 Noise	49
4.4 Scanning Artifacts and Mitigation Strategies	51
4.4.1 Beam Hardening	51
4.4.2 Metal Artifacts	54
4.4.3 Ring Artifacts	55
4.4.4 Motion Artifacts	56
5. Conclusions	57
6. References	59
7. Acknowledgements	61

# Key points/objectives:

- Introduce fundamental XCT concepts and top-level overview of advanced scanning techniques
- Demonstrate how the XCT method can be used for materials science and failure analysis applications
- Discuss common challenges and techniques to overcome them

# Glossary

**2D:** two-dimensional or planar view in which an object or cross-sectional image appears flat **3D:** three-dimensional or volumetric view through which an object or image appears with depth perception

**Artifact:** false representation or feature within the reconstructed image that does not accurately reflect a true physical structure in the object being inspected.

**Beam hardening:** Common artifact resulting in brighter edges due to proportionally higher X-ray absorption of lower energies in the outermost material. It is often reduced through adding filters to increase the average energy of the beam being transmitted through the part.

**Contrast**: Local differences in grey-level between pixels or between regions of pixels in an image (or voxels in a 3D volume). Contrast sensitivity is a relative measure of contrast between regions and relates to the user's ability to discern a feature from its surroundings.

**Geometric magnification:** The act of projecting the radiographic image such that the x-ray image transmitted through the part becomes larger with increasing magnification, enabling small features to be broadcast over more pixels (higher resolution). Magnification is a function of the spatial position of the sample relative to the source-tube distance.

**Geometric unsharpness:** Factor calculated by the focal spot size times the ratio of the sample to detector distance to the source to sample distance that governs the blurriness of the features **Latitude:** the range of gray levels present in the pixels of an image (or voxels in a 3D volume). Latitude and contrast are interrelated.

**Linear detector array:** detector that collects intensity a single line at a time rather than a larger flat panel and is often used for noise reduction for scans conducted at very high energies **Noise:** grainy image appearance often resulting from either X-ray scattering, inadequate frame averaging, or too few projections

**Phase contrast:** increase in X-ray phase shift resulting in improved edge enhancement **Reconstruction:** Process of taking the 2D radiographs and building a 3D volume. Artifact reductions are often conducted during this stage.

**Resolution:** Size of a pixel (or voxel in 3D space) in relation to the physical size it represents on the sample. Key factor for feature detectability, often relying on both the voxel size and geometric unsharpness. In combination with contrast sensitivity, these characteristics define overall image quality. **Segmentation:** Process of defining a boundary between phases of different densities and therefore

grayscale contrast (often conducted to define the boundary between the scanned part and the surrounding air)

**Voxel:** A 3D pixel, or "volume pixel" that is the elemental measurement unit in a scan volume and a primary factor in the scan resolution and feature detectability. The voxel size is often defined as the field of view divided by the number of pixels across the detector.

# Keywords

Characterization, Failure Analysis, Image Analysis, Materials Science, Microscopy, Non-Destructive Evaluation, X-ray Computed Tomography, X-ray Imaging

## **Abstract**

This chapter provides an overview of XCT with applications and examples focused in the field of materials science. Some common advanced scanning methods and their particular advantages are discussed. Case studies are shown to demonstrate quantitative examples and failure analyses. Known XCT limitations and methods to overcome common artifacts are presented. This chapter demonstrates how XCT can be a very powerful characterization tool with numerous advantages for understanding fundamental material relationships or identification of specific location or causes of failure.

## Introduction

X-ray computed tomography (XCT) is a nondestructive evaluation (NDE) technique that utilizes a series of 2D radiographs collected over the course of a rotation to reconstruct, or build, (as illustrated in Figure 1) and subsequently display a 3D volume. Different phases of material have different X-ray mass attenuation coefficients, which result in different absorption/transmission values and different contrasts or grayscale values in reconstructed XCT data. The technique is well known in the medical field where it was first utilized. The primary difference is that the source and detector rotate around the patient in the medical field, whereas XCT laboratory scanners used in other industries tend to have control over the source, sample, and detector distances and then rotate the sample. Modern advancements in XCT technology have provided many opportunities for discoveries that were not possible in the recent past. It is important to understand some of the fundamental aspects of XCT and its history to appreciate just how far it has advanced.

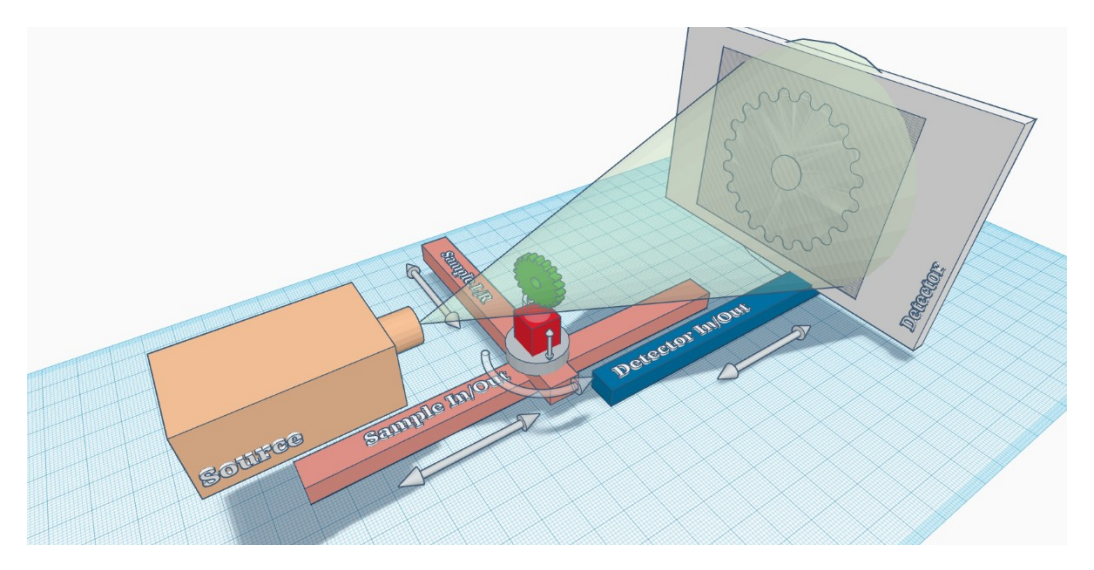


Figure 1. Schematic of XCT set up and typical motion controls

This chapter is organized into four major sections. The intent behind these sections is to offer the reader a broad overview of different aspects of XCT as an NDE method for the purposes of understanding its merits and limitations, rather than as an instructional, step-by-step guide. Section 1 summarizes XCT

fundamentals, history of its development and major advancements, and applications to materials science. The fundamentals presented in this section are defined and several are referred to in subsequent sections within the chapter. Comparisons to other NDE methods are described to better understand when XCT might be the most suitable NDE method. Additionally, this section discusses complementary material characterization techniques. Many of these are destructive techniques but are often able to provide different resolutions or other chemical or phase identification, so it is often beneficial to utilize XCT in conjunction with other techniques.

Section 2 describes several non-traditional scanning techniques that transcend beyond single, flat panel scans or volumetric computed tomography. Discussed in this chapter are the use of a linear detector array, helical scanning, dual-energy scanning, phase contrast enhancement, diffraction contrast tomography, in-situ mechanical testing or temperature-controlled scans, additional degrees of freedom for scanning complex shapes, and capturing motion or dynamic events during a scan. These techniques allow unique possibilities to reduce noise due to X-ray scattering, greatly enhance contrast between phases of similar attenuations, visualize defects that are only present during specific loading or thermal conditions, and resolve features that would not be detectable with a standard XCT scan. Additionally, advantages of utilizing iterative reconstruction versus the more traditional back-filtered projection method is demonstrated.

Post-reconstruction analyses presented in section 3 highlight a few examples of quantitative analyses and the valuable information that can be gained from XCT scans. Advanced segmentation techniques are discussed to isolate phases for further analyses. Automatic defect recognition and the implementation of machine learning algorithms demonstrate the possibilities of computerized methods to minimize time-consuming analyses conducted by personnel. Dimensional tolerance deviation analysis can quantify the accuracy of a manufactured part relative to the original drawing for quality control purposes. This technique can also quantify the extent of thermal residual stress distortions or physical deformations after mechanical testing. Porosity analysis can aid the fundamental understanding of processing-microstructure-property relationships and explanations for failure. Other failure analysis case studies discussed show rupture of a copper ground plane within the printed circuit board, a crack in an additively manufactured flow device, failed wires within a boroscope camera, and a close call mishap of an astronaut helmet. These failure analysis examples demonstrate where XCT was able to aid in the explanation for the cause of failure or identify the cause or specific failure location when other methods were not able to obtain this information.

While the many advantages of advanced scanning, reconstruction, and analysis techniques demonstrate a wide variety of materials science applications, it is important to address some of the current XCT limitations and artifacts, which are presented in section 4. Knowing some of these limitations aids in preparing XCT samples to the appropriate size, understand the practical feasibility of detecting features of a particular size, or better optimize scan settings. Knowledge of scanning artifacts helps to understand what features are real within the microstructure versus a false remnant that appears. This can be due to particular scanning conditions, inherent physics limitations, or other errors such as movement during the scan or defective pixels on the detector. A vast majority of the time, artifacts can be minimized or eliminated with modified scanning conditions or corrections during the setup or reconstruction phase.

### 1.1 XCT Fundamentals and Basic Parameters

The Beer-Lambert Law for absorption of a narrow monoenergetic beam of X-ray radiation by a material can be written

$$I = I_0 \exp[-\mu s]$$
 Eq. 1

where  $I_0$  is the initial intensity of the beam, I is the intensity of the beam transmitted through the absorbing material, s is the thickness of the material, and  $\mu$  is the linear attenuation coefficient of the material. The linear attenuation coefficient is a measure of the fraction of a radiation beam per unit thickness that a thin absorber will attenuate, including both absorption and scatter. If a 2D section through an object of interest is considered, Equation 1 can be written as

$$I = I_0 \exp[-int[\mu(x,y) ds]]$$
 Eq. 2

where  $\mu(x,y)$  is the distribution of linear attenuation coefficients over 2D space and ds is the differential of the X-ray path length through that space. Dividing both sides of Equation 2 by  $I_0$  and taking the natural logarithm of both sides yields,

$$\ln (I_0/I) = \inf[\mu(x,y) \, ds]$$
 Eq. 3

which is known as the Radon transformation of  $\mu(x,y)$  and is the fundamental physical equation of the XCT process. The quantity  $\ln(I_0/I)$  is called the projection value, P, along the X-ray path length. The inversion of Equation 3 was analytically solved in 1917, when Radon demonstrated in principle that  $\mu(x,y)$  could be determined from an infinite set of its line integrals [1]. Similarly, given a sufficient number of projection values (or line integrals) in tomographic imaging, the cross-sectional distribution,  $\mu(x,y)$ , can be estimated from a finite set of projection values [2].

The basic scanning parameters of XCT can be broken down into those of the X-ray technique and tomographic and detector settings. The X-ray technique or setup in a commercial system includes variables such as current and peak voltage (energy) of the X-ray source, focal spot size of the X-ray source (which is generally linearly proportional to the source power), additional filtering material used (if any), source to object distance (SOD) from the origination point of X-rays to the center of the specimen turntable (center of rotation), source to image distance (SID) or source to detector distance (SDD) from the origination of X-rays to the front of the detector, and the magnification, which is SID/SOD. Tomographic and detector parameters include the number of projections or views (i.e., radiographs), which directly affects reconstructed image quality, and the frame rate, number of frames to average, sensitivity, and area of use (e.g., full panel or subsection) of the detector. There are also a number of parameters used to describe and define the performance of XCT systems and in particular the capabilities of scan setups (protocols) used in the system, some of which are briefly described below.

Spatial resolution – the extent to which a tomogram (XCT slice image) or radiograph (X-ray digital radiography image) can be used to detect details of the shape of image features whose contrast is substantially greater than the image noise. XCT spatial resolution is best characterized by the point-spread or line-spread functions of the image, or by the equivalent modulation transfer function (MTF) in frequency space. The spatial resolution is generally limited by the measurement spacing, not by the spacing of the pixel grid [3].

Modulation Transfer Function (MTF) – a function giving the relative frequency response of an imaging system, in this case the spatial frequency response. The MTF is the normalized amplitude of the Fourier transform of the point-spread function [3]. The MTF is normally expressed in line pairs per unit distance at a given percent modulation of CT-density or gray level value. For example, an MTF value of 2 line pairs per mm (lp/mm) at 50% modulation basically means that features of 250 microns (1 mm divided by 4, since two pairs equals four objects) in size can be discerned from one another with a difference in respective gray levels of 50%. This is one point on an MTF curve, as modulation (difference in gray levels) decreases with increasing line pairs.

Contrast – the extent to which a parameter of interest differs for some set of features. Contrast is often stated as the percentage by which the value for one feature is greater or less than the value of the other. For example, aluminum may have a 71% XCT-density (gray level value) contrast to iron at 200 keV. Contrasts in the physical properties of different parts of an object may result in contrasts in the image densities, or gray levels, for tomograms and radiograms [3].

Contrast sensitivity (XCT density resolution) — a measure of the extent to which a tomogram or radiogram can be used to detect differences in the physical parameter mapped by the image, for features of a given size. The limiting factor in contrast sensitivity is generally the noise in the image averaged over areas of the feature size, which may vary significantly between different regions of the image. Another important factor is the contrast that the features show under the particular scan conditions for the image. [3]

Contrast resolution – the ability to distinguish between differences in intensity, or gray level value, in an image. Contrast resolution is usually measured by generating a pattern from a test object that depicts how image contrast changes as the structures being imaged get smaller and closer together [4].

Noise – the variation in a measurement (or in an estimate or image derived from measurements), such as CT-density or gray level values, when it is repeated under nominally identical conditions. Noise commonly refers to variations over time and may apply to variations of individual pixels or of collective regions. Noise is distinguished from consistent biasing effects, which are referred to as artifacts in XCT images. [3]

Signal-to-Noise-Ratio (SNR) – SNR is the ratio of the desired signal (e.g., object's gray level value) to the level of the undesirable background noise within an image. Therefore, the SNR is the result of dividing the average (mean) signal by the variation, which is the standard deviation [5].

Contrast-to-Noise-Ratio (CNR) – CNR is the ratio of the contrast, or the difference in signal intensities between any two features or areas of an image, divided by the standard deviation of the noise level in the image. Images can have a high SNR metric, but at the same time have a low CNR metric depending on what features or areas are compared [6].

An important point about these defining quantities is that they normally apply to a given XCT setup and set of scanning parameters (protocol) using a given X-ray source and detector. Different protocols using different equipment, or the same equipment in different ways, will result in different effective spatial resolution, SNR, CNR, MTF, etc.

Most commercial and industrial XCT scanner systems use the mathematical approach called filtered back projection (FBP) to process projected image data that provides intensity values and reconstruct the

2D radiographs into 3D tomographic XCT image data. This data can be virtually sliced in any direction to visualize 2D cross-sectional slices or view the full 3D solid volumes. There are other data reconstruction approaches, but FBP has traditionally been used due to its mathematical speed and ease of implementation in digital computing systems. It typically produces good image quality results in a relatively short amount of computer processing time. There are a few commercial XCT systems that offer other reconstruction methods, like iterative, as secondary options.

## 1.2 XCT History

Given the lack of computational power and that it is a major mathematical problem to invert the Radon transformation and solve for  $\mu(x,y)$  using a sufficient number of projections, the transformation remained a curiosity as a practical imaging technique at first. It was not until the advent of enabling modern digital computer technology that permitted fast solutions to be made for large, computationally intensive images that the technique was developed into a usable imaging method [7]. In October 1963, William H. Oldendorf received a U.S. patent for a "Radiant energy apparatus for investigating selected areas of interior objects obscured by dense material" [8]. The first XCT scan of a preserved human brain (7 min/frame, 5 mm resolution, 80 × 80 pixels), which took nine days, was done in 1968. The first medical XCT scan on a patient (3 mm resolution, 80 × 80 pixels), which took five minutes, was done in 1971. Godfrey Hounsfield performed research to develop the XCT technique through the Electric and Musical Industries (EMI) under the proposal, "An improved form of X-radiography", and later invented the first commercially viable CT scanner in 1972 [9]. The first commercial medical XCT scanner for inspection of the head (EMI 1000) was released in 1973, of which six models sold worldwide. The first whole body XCT scanner (EMI CT 1010) was released in 1975. In the 1980s, Feldkamp's 3D conebeam algorithm approach [10] was widely implemented and applied in volumetric, or flat-panel, computed tomography, rather than processing individual slices from a fan beam one at a time, which led to a significant reduction in computational time.

XCT scanners have advanced significantly since their initial use in the medical field and have continued to improve upon resolution limits over the past several decades. The first X-ray micro-computed tomography, or micro-CT, system was conceived and built by Jim Elliott in the early 1980s. The first published X-ray microtomographic images were reconstructed slices of a small tropical snail, with pixel size about 50 micrometers [11]. The first commercial micro-CT scanner was released in the mid-80s. Nano-computed tomography, or nano-CT, is an emerging, very high-resolution cross-sectional imaging technique and is currently the highest resolution XCT-technology available for 3D imaging. Nanoscale 3D imaging started at synchrotrons and has extended to laboratory settings [12]. Currently there are only a few commercially available nano-CT scanners, with pixel sizes and spatial resolutions on the order of tens or hundreds of nanometers, as shown in Figure 2. Typically the field-of-view able to be scanned in systems like these is tens or hundreds of micrometers. Similarly, high-energy computed tomography, or XCT that uses X-ray sources with energy of one Mega-electron Volt (MeV) and higher, is also an emerging realm of XCT scanning. Currently there are also very few high-energy XCT scanners commercially available, which are quite expensive due to their general equipment and X-ray shielding requirements.

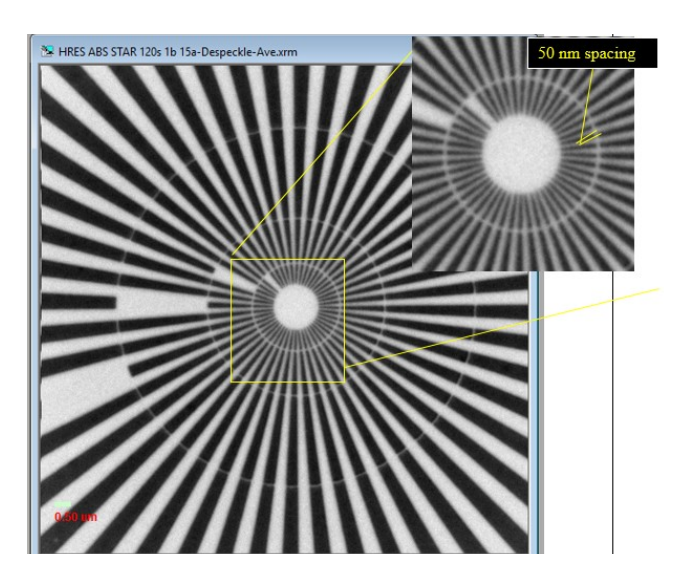


Figure 2. Demonstration of 50 nm feature detectability on a Zeiss 810 Ultra nano-CT

Since their beginning, XCT scanners have been developed in a series of major technical advancements classified as generations, which collectively describe the majority of the scan geometries that have been employed. This classification is a legacy of the early, rapid development of XCT in the medical arena, and these terms are still widely used. First generation pencil beam XCT systems are characterized by a single X-ray source and a single detector that undergo both linear translation and rotational motions, and have the disadvantage of relatively longer scanning times. The primary difference in second generation pencil beam XCT systems, which use the same translate/rotate scan geometry as the first generation, is that they use a fan beam of radiation and multiple detectors so that a series of views can be acquired during each translation, which leads to correspondingly shorter scan times. Third generation XCT systems normally use a rotate only scan geometry, with a complete view being collected by the detector array during each sampling interval, which is one complete rotation of the turntable. Typically, third generation systems are faster than their second generation counterparts. Spatial resolution in a third generation system depends on the size and number of sensors in the detector array and improvement in scanning speed is achieved by implementation of significantly more sensors than with earlier generations. Many commercially available industrial XCT scanners use the rotate only scan geometry setup, in which the object rests on a rotating turntable between a stationary X-ray source and detector, as opposed to a stationary object inside a rotating ring of source and detector like the medical practice. Thus, many commercial and industrial scanners are considered to be of the third generation type. Fourth generation inverted fan beam XCT systems also employ a rotate only scan motion, but use a stationary circular array of detectors with only the source moving. The test specimen is placed within the circle of detectors and is irradiated with a wide fan beam that rotates around the test specimen. Fifth generation cone beam cylindrical XCT systems are different than the previous modes in that there is no mechanical motion involved. The scanner uses a circular array of X-ray sources, which are electronically switched on and off, and project onto a curved fluorescent screen. To date first, fourth, and fifth generation scan geometries have seen little commercial application, but there may be special situations for which they would be well suited [13]. The cone beam irradiation method used for area image data collection by fifth generation XCT scanners is currently commonly implemented in industrial scanners using cone beam X-ray sources and solid state direct digital array (DDA) flat panel detectors. This setup is often combined with a turntable rotate only scan geometry, which is essentially the 3D or flat-panel volume computed tomography version of third generation scanning. Originally, third generation scanning only used a straight or curved multi-element linear detector array. Advancements in XCT systems technology and methodology, including X-ray sources, X-ray detectors, scanning geometries, computer hardware and software, and XCT reconstruction approaches, will continue as scientists, engineers, and various commercial and medical entities further develop the expanding areas of XCT testing, analysis, and evaluation.

## 1.3 Materials Science Applications

Since its development in the 1970s, XCT has proven to be a versatile imaging technique in numerous industries. The XCT technique is a widely applicable and powerful nondestructive inspection modality for evaluation and analysis of geometrical and physical characteristics of materials, especially internal structures and features. XCT is applicable to metals, ceramics, plastics, and polymer, metallic, and mixed composites, as well as components, assemblies, and materiel. The principal advantage of XCT is that it provides densitometric (that is, radiological density and geometry) images of thin cross sections through an object in a noninvasive manner. Because of the absence of structural superimposition, images are much easier to interpret than conventional radiological images. The user can quickly learn to read XCT data because images correspond more closely to the way the human mind visualizes 3-D structures than 2-D projection radiology (that is, film radiography, real-time radiography, and digital radiography) [3]. Also, unlike a number of other nondestructive testing modalities, XCT does not require a transfer medium or close proximity between specimen and probe (X-ray source) and the specimen's overall shape, geometric characteristics, and surface roughness generally do not preclude application of XCT.

In general, XCT is used to detect a wide variety of surface-connected and internal discontinuities and flaws in materials, including density variations, cracks, shrinkage (cavities), voids, porosity and microporosity/nanoporosity, laps, inclusions, foreign objects, impurities, segregation, bond separation, missing parts, part misalignment, and service degradation, as well as thickness and dimensional measurement, flaw distribution, chemistry variations (limited extent), and elemental distribution (dual energy XCT) [7]. XCT has proven to be an invaluable, multi-disciplinary tool for quality control, part inspection, and failure analysis. Having the ability to simultaneously search both the exterior and the interior of a part, non-destructively, for various sorts of defects is pivotal. While other NDE techniques may offer advantages in particular cases, XCT offers an unmatched versatility to a wide array of materials, defects, and applications. Furthermore, because XCT images are digital, they may be enhanced, analyzed, compressed, archived, input as data into performance calculations, compared with digital data from other nondestructive evaluation modalities, and transmitted to other locations for remote viewing and more advanced analysis [14]. Key industrial applications where XCT has proven extremely valuable are in the areas of rapid prototyping, reverse engineering, and metrology. Rapid prototyping can be accomplished utilizing a class of manufacturing techniques where parts are built from computer models in a variety of materials. Stereolithography is one such technique that can use the information of XCT to produce extremely accurate polymer parts. XCT-assisted reverse engineering methods are successful in enabling older designs without computer aided design (CAD) files to access the many rapid tooling techniques currently available. There are many computational methods that allow the XCT-derived digital data to be transformed to CAD contours, which can be used to reverse engineer the part of interest. Given the dimensional capabilities of current XCT scanner systems, XCT data is similar to dimensional data from coordinate measuring machines except that it provides a number of advantages—XCT data is acquired without contacting the part and XCT data not only provides surface information but also accurate measurements of all internal structures, regardless of its structural complexity. Metrology of XCT data, which is the evaluation of dimensional measurements, can be accomplished using a number of techniques. The most accurate means is by reverse engineering the XCT data, which normally requires the generation of a point cloud—a collection of points in 3-D space that represent the surface of the part determined from the XCT data. The deviations between the inspection data and the design data or CAD file are often evaluated based on the necessary tolerances for the application [13]. This type of application of XCT data is often generally called a nominal (design) versus actual (inspection) comparison, which is commonly used to aid in the evaluation of rapidly prototyped, first article, or other initially fabricated or produced materials or components. Of course, this approach can also be utilized after any type of testing or damage, assuming that the material or part is not completely destroyed in the process.

XCT affords extensive capabilities for a variety of applications and provides an ideal examination technique whenever the primary goal is to locate and size planar and volumetric features in three dimensions. In addition to a nondestructive inspection technique for quality control, XCT data at its core is a record of the density differences present in a material or part/component and feeds into other programs to provide rapid prototyping, reverse engineering, metrology, and nominal versus actual comparisons capabilities, as well as quantitative calculations of feature or flaw sizes, shapes, and distributions. The ability of an XCT system to provide non-superimposed cross sectional areas of interest through an object makes it a powerful complement to conventional radiographic inspections, and, when used in conjunction with other NDT methods, such as ultrasound, XCT data can provide unique insight into material integrity.

## 1.3.1 Comparisons with other NDE methods

Nondestructive evaluation methods can be described by their basic physical principles and how they probe or interrogate materials to detect discontinuities. Nondestructive testing (NDT) categories can be broken down into mechanical-optical, penetrating radiation, electromagnetic-electronic, sonicultrasonic, thermal, and chemical-analytical techniques, with auxiliary categories of image generation and signal-image analysis techniques [7]. The techniques in each category are generally defined by their physical processes and basic test result, as well as the key material property or properties that affect the process and produce different test results. For example, in X-ray radiography (film), digital radiography, fluoroscopy, and XCT a portion of incident X-rays of a given energy and intensity pass through the object being tested and are then recorded in some fashion. The differences here are in how the X-rays are generated and recorded. The key material properties are attenuation coefficient (i.e., atomic cross section or mass coefficient) and density, since both exponentially affect the transmission of X-rays through the object. In the case of ultrasonic testing, sound energy of a given center frequency (from kilohertz to a hundred MegaHertz range) is generated and directed into the object being tested, usually using some form of couplant medium between the ultrasound generator (transducer) and the object. Air coupled, or no couplant, ultrasonics using relatively very low frequencies have been developed. The speed of sound is different in different materials and the center frequency of the transducer determines the wavelength of the longitudinal sound waves in the material. In ultrasonic testing the key material property is acoustic impedance and differences in impedance between materials, e.g., a metal and the air or gas in a void, determine how ultrasound energy is transmitted and reflected at material interfaces.

Another way to think about NDT categories is in terms of those most used for commercial and/or industrial uses: X-ray radiography/digital radiography/XCT, gamma radiography, ultrasonic testing, electromagnetic eddy current testing, magnetic particle testing, and liquid penetrant testing. In addition, thermal testing (aka, thermographic imaging) and microwave testing, albeit likely less than the others, are also currently used commercially and in industry for some applications. This is by no means an exhaustive list. However, it does allow for some general comparisons between these main NDE areas. For example, among this list of the more common industrial NDE techniques, only the X-ray, gamma ray and ultrasonic techniques generally provide the capability to inspect the whole interior of an object, also known as volumetric inspection. Certain types of thermal and microwave or terahertz testing provide some capability to inspect the interior of objects. The other techniques are commonly used to inspect for near or very near surface and open to surface discontinuities. X-rays are highly attenuated by heavy, dense materials like high density metals (e.g., steel, nickel, and copper), although higher X-ray energies can be used to increase penetration, usually at the expense of beam focus and image sharpness. Ultrasonic techniques are not affected this way by heavy, dense materials, although air content and materials which effectively scatter ultrasound energy, like certain composites, severely limit penetration. Penetration of ultrasound into matter is in part dependent on frequency, with higher frequencies being less penetrating. Eddy current techniques require the test object to be an electrical conductor. Magnetic particle techniques require the test object to be ferromagnetic, i.e., it must be able to be magnetized, unlike aluminum for example. Microwave techniques cannot inspect solid metallic objects as microwaves are reflected by metallic surfaces, although they can be used to inspect for discontinuities in metallic surfaces or disparate metal objects in non-metallic matrices or materials in some cases. Similarly, terahertz (which lies between microwave and infrared frequencies) spectroscopy or imaging may be used for volumetric inspection but is most advantageous for NDE of non-metallics and porous media such as foams. Thermal imaging techniques require the test object to be a thermal conductor and the time scales of both heat transmission and dissipation must be considered. Here, in-plane diffusion may compete with the through-thickness diffusion, often obscuring the thermal response from progressively deeper features. Shearography is a unique NDE technique that is particularly useful for detecting near or sub-surface air gaps (such as pores, disbonds, delaminations, etc.) in multilayered material such as composites or coated surfaces.

Neutron radiography, including neutron CT (sometimes called "N-ray CT"), is quite similar in a lot of ways to X-ray radiography and XCT. The key difference between these techniques lies in the interaction physics between the materials and the radiation. The X-ray photons in XCT interact with an atom's electron cloud, whereas neutron particles interact with atomic nucleus. Thus, attenuation cross-sections are very different and X-ray absorption tends to scale, roughly, according to an element's periodic number, whereas neutron absorption does not. Neutron radiography is accordingly very useful for detection of certain elements, for example hydrogen, and is not significantly attenuated by most industrial metals. It may be particularly useful therefore for inspection of o-rings, gaskets, or grease within a large metal structure, though it suffers from being a far more limited-use technique since neutron generation generally requires a nuclear power reactor. XCT can be useful for similar situations, but its industrial effectiveness is much more dependent by the type of alloy and thickness. XCT is much more common technique for NDE applications, mostly due to its advantages in finding defects in a wide range of materials including metallic structures, plus the relative ease of creating x-rays safely in a common, controlled laboratory environment.

This discussion shows that no one NDT technique or set of methods can detect every type of discontinuity or flaw in every kind of material or object. However, certain NDT techniques can be used together to synergistically complement one another in some cases. For example, this is the case when using 2D digital radiography, and to a lesser extent XCT, and ultrasonic testing to inspect an object for discontinuities, including laminar features with surfaces perpendicular to the X-ray beam. Since X-ray radiography and XCT depend on differences in linear attenuation over space at a given spatial resolution to detect discontinuities, it can be problematic to detect tight cracks, "kissing" disbonds, and other features without discernible physical separation in like materials. For radiographic methods to be helpful in detecting cracks (particularly with 2D radiography), the X-rays generally need to be oriented along the direction of the crack for there to be enough of an "air gap" along the line of sight of the X-ray beam for it to equate to a drop in overall transmission. To this end, X-ray radiography for crack detection is most useful when one has some expectation of the direction in which cracks are expected. In these cases, it may help to supplement an X-ray inspection with ultrasonic testing. Because of the nature of ultrasonic sound reflection and transmission at dissimilar material boundaries (i.e., acoustic impedance mismatches), ultrasonic techniques can be and often are better at detecting these types of discontinuities. The dissimilar material that causes reflection of ultrasound in a kissing or relatively small gap disbond is often air, and very little air is needed to cause an appreciable impedance mismatch, making ultrasound very effective for these types of flaws. Conversely, this sensitivity to air or to dissimilar material interfaces can often make ultrasonic testing less effective in certain materials. In these cases, X-ray radiography may be used as a useful supplement if one is inspecting for voids, foreign object debris (FOD), or other features embedded within the material.

## 1.3.2 Complementary materials characterization techniques

Other materials microscopy characterization techniques such as optical, scanning electron, transmission electron, confocal, and atomic force microscopy can be advantageous to achieve higher resolution results or additional information that cannot be obtained through XCT alone. X-ray energy dispersive spectroscopy (XEDS) in the scanning electron microscope (SEM) is beneficial to identify specific elemental compositions that cannot readily be identified in XCT without additional calibration scans using a phantom. Therefore, the XEDS is often used in conjunction with XCT for faster identification of unknown phases, while the XCT provides the benefit of full 3D volumetric information whereas the SEM is limited to surface imaging.

Confocal microscopy can provide information regarding a material's surface roughness more readily than XCT and is often a much faster method to obtain results. The technique, however, is limited to external surface morphology. This method works very well for simple geometries, but more complex designs might require XCT scanning to fully capture the part geometry. Similarly, larger scanning methods such as structured light imaging, extended depth of field imaging, structure from motion, and photogrammetry methods may also work well to generate 3D models or dimensional metrology measurements as long as the surface can be captured within the line of sight with the laser or light source.

The primary advantage for XCT over many traditional materials characterization methods is the ability to capture full 3D microstructural information, whereas a majority of other microscopy methods are either 2D imaging techniques or require destructive methods such as serial sectioning in order to capture a larger volume. The serial sectioning can often be very time consuming and/or labor intensive. Additionally, the control of material removal rate and the ability to accurately measure the layer depth can be challenging when using manual polishing methods [15, 16]. Automated or robotic serial

sectioning methods are much more accurate, although they can also be expensive and time consuming to implement.

# 2. Advanced Scanning and Reconstruction Techniques

Table 1 describes the advanced scanning techniques described in this section and their primary benefits. More details about each particular scanning technique are discussed in more detail in the sub-sections, often with materials science relevant examples, illustrating the improvements made through the utilization of these techniques.

Table 1. Summar	v of advance	d scannina ti	echniques i	and their	nrimary he	pnefits
Tubic 1. Julilliai	y of advance	a scarring to	cciningacs	arra cricii	pillially be	,110,110

Scanning Technique	Primary Benefits			
Linear detector array (LDA)	Noise reduction for high energy scans			
Helical	Tall, narrow geometries or reduction of cone- beam artifacts			
Dual energy	Segmentation of phases of similar attenuations, particularly of higher densities			
Phase contrast	Increased edge detection for low absorption materials			
Diffraction contrast	Grain size and orientation			
Open CT	Additional geometry flexibility, especially for target areas on a complex shape or limited access			
Static CT	Significantly reduced scan time			
Cryogenic or temperature-controlled CT	Capture microstructures at hot or cold temperatures, assess cold-induced failure mechanisms, or map internal 3D strains or expansion coefficients			
In-situ mechanical testing	Defects present during compression or tensile loading			
4D scanning	Dynamic motion (at compatible timescales)			
Iterative reconstruction	Improved image quality (noise reduction, sometimes improved contrast); less scan time in certain cases			

## 2.1 Linear Detector Array

There are two primary types of detectors used for data acquisition: flat panels for volume-based XCT scanning and linear detector arrays (LDA) for data collection of a single horizontal line of pixels at a time. Essentially most, if not all, commercial XCT scanner systems that use a flat panel area detector for volume-based XCT employ the 3D cone beam algorithm of Feldkamp [10], which is a straightforward extension of the single slice 2D algorithm that has been used for decades in X-ray fan beam based systems, to reconstruct projected area data. The speed, efficiency, X-ray energy range, resolution, artifacts, noise, and scatter-rejection capabilities of systems utilizing cone beam methods can differ substantially from systems using fan beam methods based on LDAs [3]. Volume-based XCT has the distinct advantage of fitting an entire object within the field-of-view (FOV) of the cone beam and collecting projection data throughout the entire volume of the object during one 360 degree rotation, unlike single slice fan beam XCT. Thus, the use of flat panel detectors provides a relatively large area for

scattered X-rays to enter the detector and uses the available X-ray flux significantly more efficiently, drastically speeding up the inspection process. However, scanning with a flat panel detector can have its own limitations, including fundamental geometric limitations due to the size of the cone beam and magnification. Secondly, it can be very difficult, if not impossible, to get good quality results from relatively high energy scans of heavy, dense, and thick or complex materials, which highly attenuate and produce significant X-ray scatter. This is usually due to a combination of X-ray starved paths through the test object and X-ray scatter contributions to the XCT data due to Compton scattering. Any scattered X-rays that enter the detector increase noise, decrease SNR, and degrade reconstructed image quality.

The deleterious effects of certain high energy scanning issues can be mitigated to an extent by using materials to "harden" the beam at the X-ray source and/or filter the attenuated beam before the detector (as discussed in more detail in Section 4.4.1). However, sometimes flat panel XCT results are just not sufficient and it is significantly better to utilize a combination of an LDA and some form of collimation at the X-ray source to reduce scatter. An LDA is a constructed 2D array of detector elements, often scintillator and photodiode-based, positioned side by side in a straight or curved shape, which is used with a collimated X-ray fan beam (horizontal) architecture. The X-ray source and LDA, which is collimated to a thin slit, are kept optimally aligned across from one another during the scan and spatial resolution is dependent on the center to center spacing or pitch of the detector elements in the LDA. The LDA does not detect any X-rays scattered out of the plane of the fan beam, which maximizes information from straight X-ray paths and greatly reduces noise contributions from scattered X-rays. The use of an LDA also eliminates the presence of the cone beam coming into the field of view of the flat panel detector, as well as likely reduces "material burnout" or "missing material" effects or artifacts in some high energy XCT scans of highly attenuating and X-ray scatter producing objects. Figure 3 shows 3D volume renderings from both a conventional flat panel XCT scan on the left and an LDA XCT scan on the right of a high density nickel turbine blade. The improvement in the image data from an LDA-based scan is apparent and the volume can readily be segmented without deleting thin walls of the structure or erroneously including external scatter. Of course, the drawback to utilizing an LDA and X-ray fan beam setup or architecture is scans take significantly longer compared to flat panel scans, since XCT projections are being collected one slice at a time. Thus, the pros and cons of using a flat panel versus LDA, including material density, scan time, features of interest desired to be detected, and the likely set of scanning parameters or protocol all need to be considered when deciding on the most appropriate XCT technique.



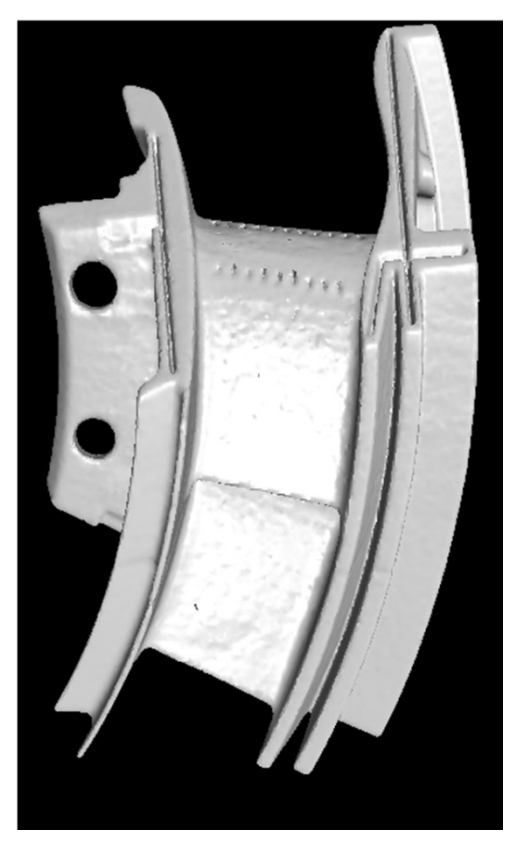


Figure 3. 3D surface renderings generated from conventional XCT scan using a flat panel detector (left) and LDA scan (right) demonstrating the improvement in the ability to segment thin-walled features (indicated by the red circle) without excess noise due to high energy X-ray scattering

## 2.2 Helical Scanning

Helical scanning is a method of continuous data acquisition as the source and detector move in alignment simultaneously from one end of the object being scanned to the other. One primary advantage of this technique is the ability to achieve higher magnification on a tall, slender object within a single scan. Imagine scanning an object such as a baseball bat. The height of the bat would significantly limit the geometric magnification if conducting a single flat panel scan, but the scan width is the dimension that governs the pixel size due to the sample width and the number of pixels across the detector. Using helical scanning, the field of view can be optimized so there is less air surrounding the sides of the bat (i.e., higher geometric magnification), thereby maximizing the achievable resolution. Then the combined vertical movement of the source and detector during acquisition captures the entire volume of the bat.

Another advantage of helical scanning is direct alignment of the source and detector with every position through the height of the sample. This is demonstrated in Figure 4 with a stack of compact discs (CDs). With the traditional cone-beam or flat panel XCT scanning (Figure 4B), only the gaps between CDs can be seen towards the center of the scan. Figure 4A, however, shows separations between discs throughout the entire stack. This is because the coning artifact in flat panel XCT distorts features in directions parallel to the axis of rotation (up and down) away from the effective position of the central slice of the rotation, due to the lack of X-ray paths that are parallel to features away from the central slice. This leads to a loss of spatial resolution along the axis of rotation away from the central slice,

which becomes more severe the farther away any part of the object is from the central slice [17]. This technique is important for detection of discontinuities like cracks that are oriented radially from the scan rotation axis and laminar features with surfaces perpendicular to the scan rotation axis, especially relatively far from the central slice.

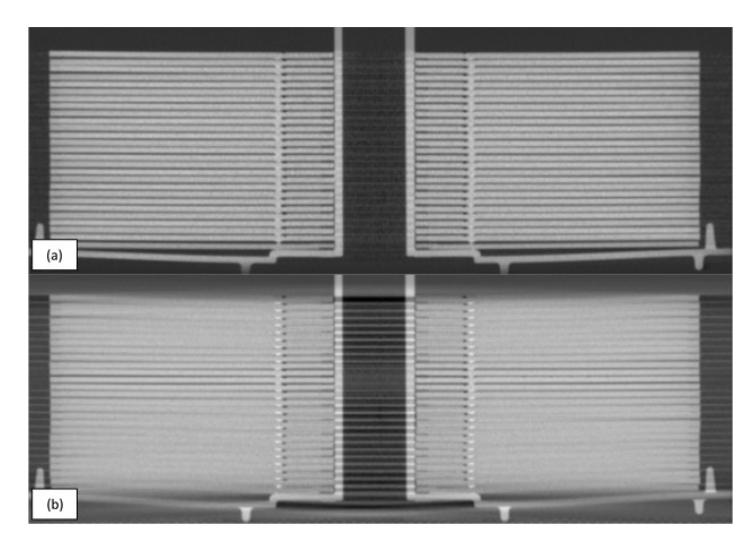


Figure 4. Scanning a stack of CDs A) with helical scanning shows a clear separation between every disc through the entire height and B) traditional cone-beam scanning only shows separations at the center of the sample (Image provided by NorthStar Imaging, Rogers, MN)

## 2.3 Dual Energy Scanning

Dual energy XCT scanning can be used to increase contrast between phases of similar attenuations. This is primarily due to the difference in the dominating photon interaction mechanisms at different X-ray energies as well as the average atomic number and density of the material. Lower X-ray energies less than are predominantly dictated by the photoelectric effect and higher energies are governed mostly by Compton Scattering. The transition point has been reported to be approximately 100 kV [18], although the transition point is highly dependent on the specific atomic number and density of the material and can vary widely. There are multiple ways dual energy scanning can be implemented. Some systems have two X-ray tubes mounted at a rotation angle of approximately 90 degrees from one another, which allows for simultaneous data acquisition. Another method employs a multi-layered detector with the low energy data collect in front while the higher energy data is transmitted through the front detector to reach the detector behind it. A different technique utilizes rapidly alternating X-ray energies between low and high voltages during the course of a single scan. This method requires a specialized X-ray source to adjust the energy level in less than one millisecond and often results in a high noise level in the lowenergy data [19]. Alternatively, two consecutive scans at different energies can be conducted and merged after reconstruction. Although this takes more time, the technique works well for non-medical CT applications where there is not a need to limit patient dosage.

In general, lower energy scans have improved contrast between phases of different densities due to larger differences between the attenuation coefficients [20]. Some material combinations are particularly challenging, and one of those combinations is aluminum and silicon carbide (Al-SiC). There is only about a 7–8% difference in the linear attenuation coefficient between these materials and the attenuation coefficients remain close at various energies [21]. Figure 5 is a plot of the mass attenuation

coefficient as a function of X-ray energy for both Aluminum and Silicon according to the National Institute of Standards and Technology (NIST) Standard Reference Database 126 [22]. This database can be used to compare differences in material attenuations at various energies to optimize the scanning voltage and enhance contrast between phases. This is particularly useful if materials have different K-edge absorptions, which is a sharp change in the attenuation at a specific energy based upon the binding energy of the K-shell electrons.

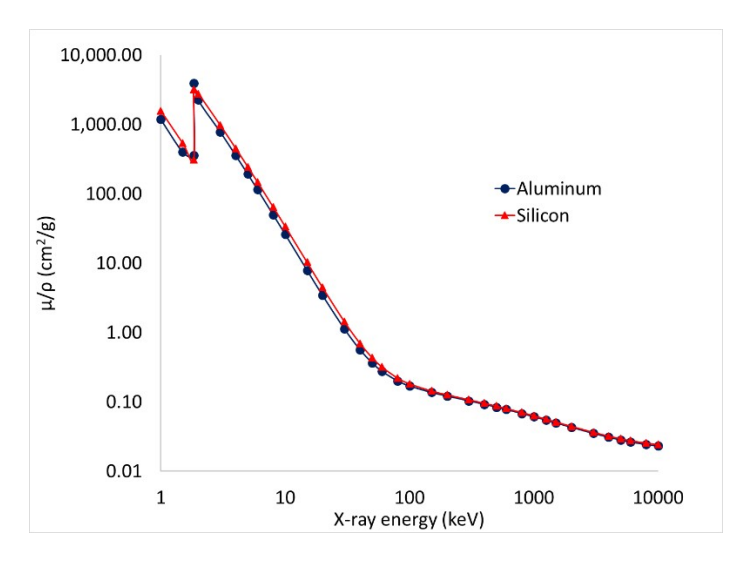


Figure 5. Aluminum and Silicon mass attenuation curve generated from the NIST database [22]

As seen in Figure 6, there is very little contrast between the SiC shells and the aluminum matrix (SiC shells highlighted by the red dashed lines in the right image). This makes it very challenging or impossible to segment the phases for subsequent volume renderings or data analysis.

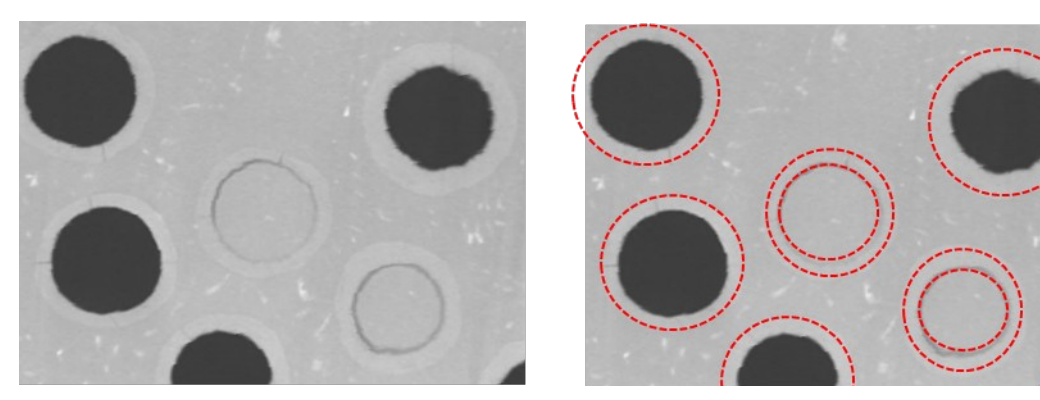


Figure 6. Al-SiC composite showing aluminum matrix (background) and SiC shells with very little contrast due to the similarity in attenuation coefficient A) raw grayscale image and B) red dashed lines to show the location of the SiC shells

The Al-SiC composite was scanned with a low energy of 40 keV and no filter (photoelectric effect regime) and again at a higher voltage of 150 keV with a thick filter (Compton scattering regime). The filter is used to increase the average energy of the beam since it is a polychromatic source (filtering is discussed in more detail in Section 4.4.1). Figure 7A-B shows cross-sectional images of the low and high energy scans. The datasets were aligned and registered so the same features were located at the same positions, and an intensity histogram was generated of the high energy versus low energy grayscale values and their frequencies. Clusters within the 2D histogram indicated different phases, which was used for

segmentation. Figure 7C shows the SiC phase that was successfully isolated from the aluminum phase through the application of dual-energy scanning.

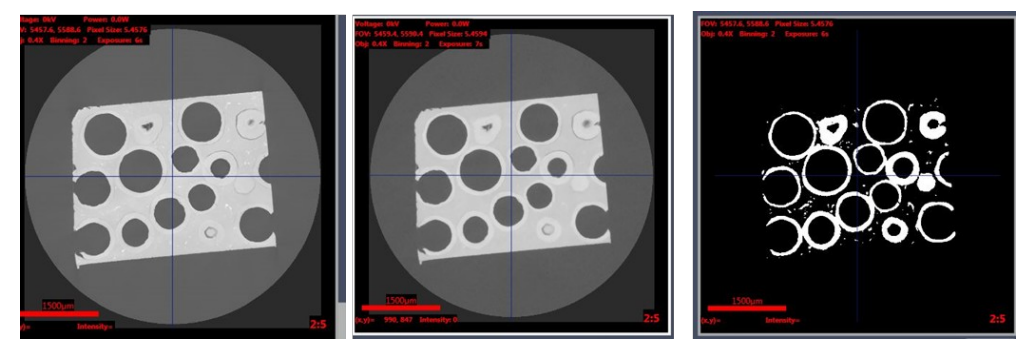


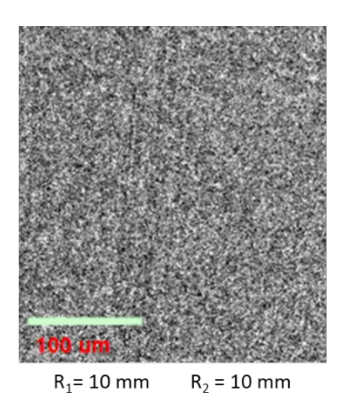
Figure 7. Dual energy segmentation of aluminum and SiC phases: A) low energy scan, B) high energy scan, and C) successful segmentation of the SiC phase

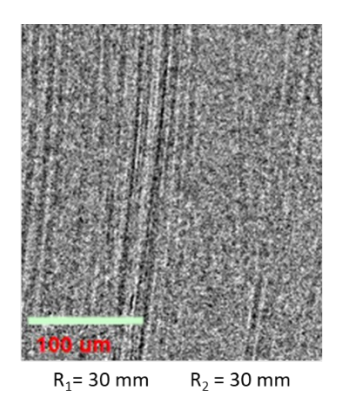
### 2.4 Phase Contrast

Phase contrast methods are particularly useful for enhancing edges and are a highly complementary technique when used in conjunction with absorption-based imaging, especially for laboratory-based scanners rather than synchrotrons [23]. There are numerous techniques to increase contrast in X-ray images, and these have already been well summarized in the literature. Chen et. al. provides a nice description of several phase contrast methods, including: X-ray crystal interferometry, diffraction enhanced imaging (also known as analyzer-based imaging), in-line holography (also known as propagation-based imaging), coded aperture X-ray imaging, and grating-based interferometry [24]. It is well known that low density materials benefit most from phase contrast imaging methods due to their low absorption.

The in-line or propagation-based phase contrast method is readily implemented on commercial scanners since it does not require the incorporation of additional hardware or software. This technique is primarily governed by increasing the refraction of X-rays through increasing the sample to detector distance in particular. A larger distance between the sample and detector results in an increased phase shift of the X-ray wavefront, leading to Fresnel fringes prior to reaching the detector. The extent of phase contrast enhancement is mathematically described through the equation:  $R_1*R_2/(R_1+R_2)$ , where  $R_1$  is the source to sample spacing and  $R_2$  is the sample to detector spacing.

The in-line phase contrast is demonstrated in Figure 8 using IM7 carbon fibers within an epoxy matrix. The left image is a 2D projection with  $R_1$  and  $R_2$  spacings of 10 mm. The image appears very noisy and it is not clear that there are any fibers present. Increasing the distances to 30 mm shows the carbon fibers, but the image still appears very noisy. Increasing further to 40 mm shows the edges of the carbon fibers very well. It is important to note the exposure time increase with the increased distances. It is well known that the X-ray intensity falloff follows the inverse square law of one over the distance between source and detector squared (1/distance<sup>2</sup>) for a point source. Therefore, increasing the distances to improve edge detection and phase contrast significantly increases the required exposure time per projection in order to achieve adequate signal intensity. This makes it impractical in some cases to conduct a full 3D scan with a high level for phase contrast enhancement.





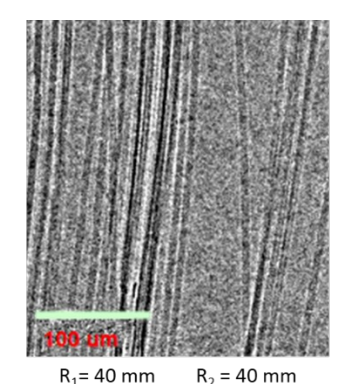


Figure 8. Demonstration of phase contrast enhancement of carbon fibers in an epoxy matrix through increasing the source, sample, and detector distances to increase the refraction phase shift

## 2.5 Diffraction Contrast Tomography

Diffraction contrast tomography (DCT) incorporates special apertures to obtain diffraction patterns and, therefore, grain information with the right sample conditions. Absorption-based imaging does not provide information regarding grain size or orientation, which are known to significantly influence a material's response and behavior in polycrystalline materials. Diffraction-based methods for 3D grain mapping were first implemented at synchrotrons, and the technology has recently transitioned to select lab-scale XCT systems.

The technique utilizes a specialized aperture between the X-ray source and sample as well as a beam stop between the sample and detector. The source, sample, and detector spacings are set up in the Laue geometry for acquisition of absorption data and diffraction data in sequential scans. Friedel pairs and axial symmetry information are used to identify the diffraction pairs and their angles. Algorithms are then used in an iterative process to build grain maps based on the indexed data. The results include grain size, orientation, and inverse pole maps. This information is similar to data collected using Electron Back Scatter Diffraction (EBSD) within a Scanning Electron Microscope, but the DCT method extends to 3-dimensions without the need for destructive slicing.

Several successes of DCT applications for materials science have been presented in the literature, including sintering of copper powder, grain morphology of aluminum, recrystallization in steel, and sodium chloride [25]. The DCT method has been validated independently with synchrotron phase contrast tomography or EBSD with serial sectioning [26, 27]. There are several limitations to the method, including sample size, minimum detectable grain size, and crystal structures, but the technique is rapidly advancing to image larger, more complex crystal structures or smaller grain sizes.

Figure 9 shows an Aluminum 4-weight percent (4wt%) Copper sample, cut into a dogbone geometry with dimensions of 1.25 mm height, 1 mm width, and 0.5 mm thickness. The sample was scanned in the Xradia CrystalCT instrument, which implements the DCT approach using a polychromatic divergent X-ray source and a flat panel detector. A helical phyllotaxis high aspect ratio tomography scanning mode was used, which is an extension of the traditional circular rotation scanning mode to accommodate larger samples and increase throughput. The color-coding of the grains refers to inverse pole figure crystallographic orientation, and the background image is an example of a single diffraction pattern collected during the acquisition.

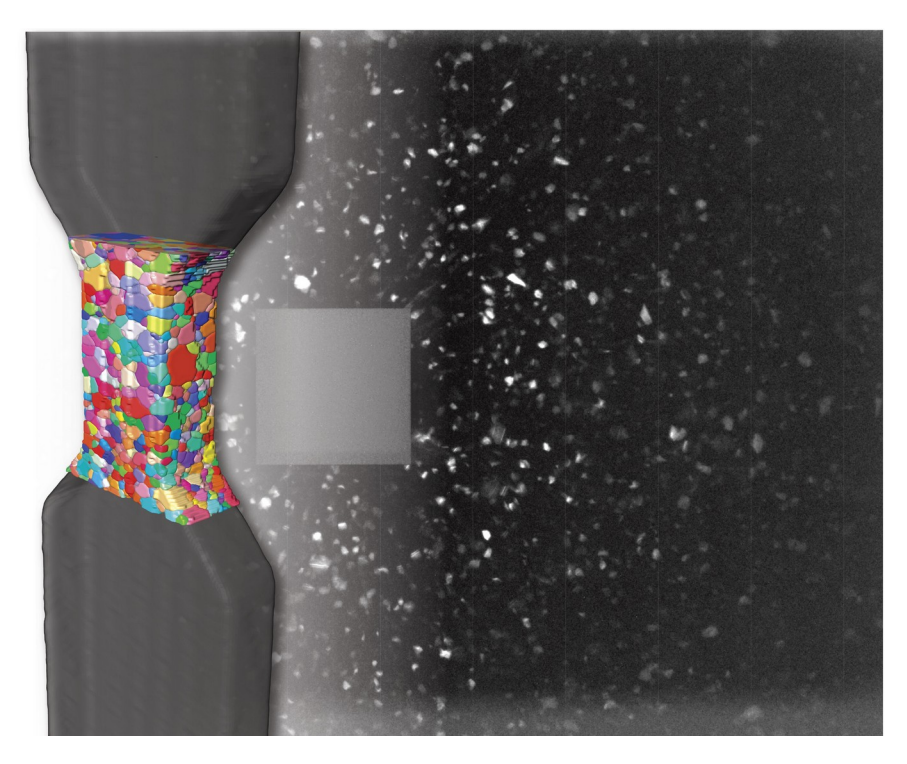


Figure 9. Al-4wt%Cu sample with inverse pole figure crystallographic orientations (colored grains), beamstop (gray colored square), and diffraction pattern satisfying the Bragg conditions (small white spots dispersed across the detector); Figure printed with permission from Carl Zeiss Microscopy and Professor Masakazu Kobayashi, Toyohashi University of Technology, Japan

## 2.6 Open CT

There has been considerable interest over recent years with the idea of a computed tomography hardware configuration in which there is no permanent frame of reference during acquisition, meaning the rotation axis and relevant spacings between source and detector are not permanent. This would be beneficial particularly for larger parts in situations in which there is limited or difficult access to the scan area of interest. There are several ways of implementing the idea and much of this is still in early stages of development. One such approach is to use a pair of robotic manipulators (such as 6 degrees of freedom [DOF] robot arms) in an arrangement in which one holds the detector and the other positions the source, then they rotate about the object of interest in tandem. This synchronized motion is captured by encoders so that the 3D positioning is saved, as well as the axis of rotation. An interesting adaptation of this method has been demonstrated for equine imaging applications, such as XCT scanning of a horse's leg [28]. Another potential variation on this concept is to have a fixed source and/or detector with a single 6 DOF robot arm. The robot arm then could retrieve the sample from a holding position, move it into the proper scanning space (and proper magnification) and then also provide the scan rotation via an end effector [29]. These configurations in essence replace the conventional translation stages in an industrial XCT system with more versatile robots and a different way to capture the critical positional data from the scan; however, the reconstruction algorithm itself remains the same. Also, in these cases the frame of reference between source and detector can be modified from scan to

scan, but it is fixed during the scan itself. More recently there has been progress toward a non-fixed frame of reference reconstruction algorithm that does not require a constant frame of reference between source and detector. This concept, analogous to the Structure from Motion (SfM) technique for 3D surface imaging, is intended to allow captured frames from any available position/orientation of the source with respect to the detector. This would enable scanning of objects in hard to reach areas, or possibly regions of interest on a part with limited access due to other nearby obstructions [ (US Patent No. 10,096,148, 2017) (J.T. Case S. K., 2021)]. While not conventional through-transmission CT, another relevant method is the Compton Backscatter Computed Tomography. This is a single-sided scanning configuration that employs backscatter X-ray and a scan sweep over the surface of interest of something less than 180 degrees. One application for this approach was demonstrated under a NASA small business innovative research (SBIR) contract for the purpose of assessing micro-meteorite orbital debris (MMOD) for applications such as space stations, habitats, etc. While it does not offer the resolution of conventional through-transmission techniques, it plays an important niche role for applications such as large flat panels or where the back side of the inspection area is inaccessible [30].

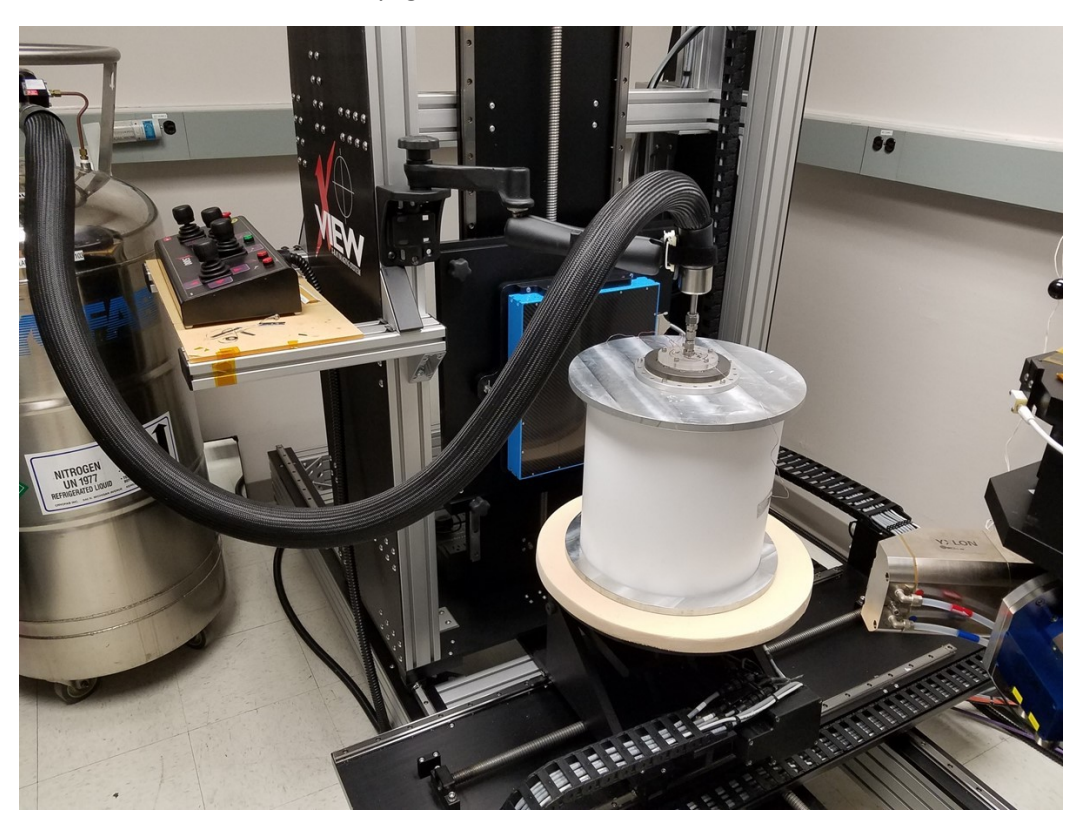
### 2.7 Static CT

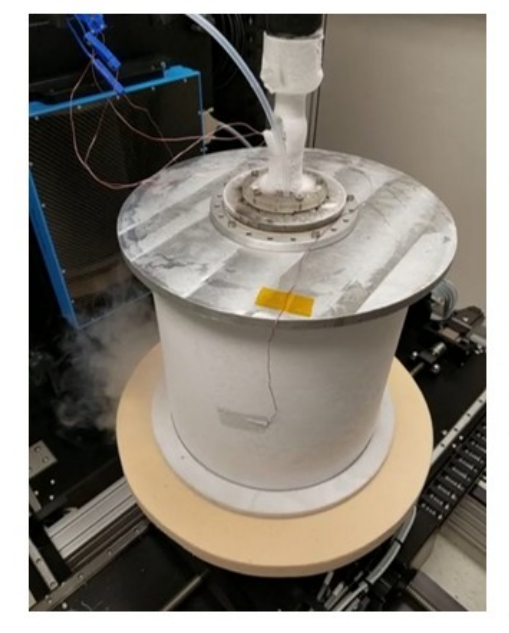
Yet another approach that involves a non-traditional industrial XCT captured geometry is the concept of "Static" or a scan with no moving parts. This implementation was demonstrated by Cramer et. al. [31] and takes advantage of miniature X-ray source technologies. Rather than a single X-ray generation source and motion control hardware to achieve different projection angles, those angles are achieved through the use of multiple, perhaps hundreds of miniature X-ray sources oriented in a ring around the object. This particular team demonstrated this concept using novel X-ray sources that are modulated using light-emitting diode (LED) stimulation of a photo-emissive film, then amplified via an electron multiplier device (as opposed to a prototypical filament type X-ray tube). These could then be rapidly turned on and off and synchronized. While there are a number of challenges and limitations with this approach, early demonstrations show great potential for an extremely rapid scan acquisition that not only saves time but could drastically limit the exposed dose. Larger scale, multiple source, and detector combinations have also been implemented to image high-speed, dynamic events [32].

## 2.8 Cryogenic or Temperature Controlled CT

A handful of commercial "environmental chamber" systems are available, as well as novel systems developed for various government, academic, or industrial labs that can expand the capability of a conventional XCT system. These include chambers to alter the temperature, apply vacuum, or expose the part to other environmental conditions (humidity, other gases, etc.). One widely applicable example is a cryogenic chamber to cool the part, often relying on some conductive conduit between the sample and cold source, as shown in Figure 10. Peltier-type cooling mechanisms are a common approach. These differential thermoelectric devices, sometimes in combination with resistive heating elements, can be used to cool or heat the sample, though they can be limited in available temperature range. Cryostats, using a liquid nitrogen or helium cooled copper base, may offer a better range of temperatures though impose a more elaborate setup with more complicated integration into the XCT chamber. The other limitation with these conductive cooling devices is that the sample itself will have temperature gradients from the top to the bottom of the sample. These stages are generally quite small and so there are sample size limitations. Also, the approach works best (though not exclusively) on samples that are more thermally conductive and have a somewhat flat base (to aid conduction). One advantage to these devices is they can be easily equipped to work under vacuum (if not inherently so), so sample cleanliness

can be maintained. (Often too, the vacuum itself can be useful, particularly with some electronics components that may fail under vacuum, or space applications.) Another approach is to use an immersive environment with liquid (or gaseous) nitrogen or helium flowing in a bath around the sample and convective currents to help maintain a more uniform temperature distribution [ (Report number 153592604, 2022)]. This approach enables cold XCT scanning of much larger objects, with no limitations on material type or geometry, though due to the convective currents, it is not ideal for samples that are very delicate. One obvious challenge in all these systems is how to integrate the cooling device with the existing XCT system. Commercial systems are designed in a compact form factor and typically adapted for a specific XCT system or rotation stage. This challenge of adaptation to the XCT system is easiest for thermoelectric cooling wherein only power connections are needed. In the case where  $N_2$  or He liquid/gas is used, care must be taken to ensure that the cooling lines do not impede/alter the motion of the stage and do not limit the needed magnification or scan rotational sweep. In the case of large cooling systems, a special type of slip ring system can be an effective approach to allow the XCT stage to rotate under or above fixed cryogenic feed lines.





# Cold scan done on Al foam sample at -100C.

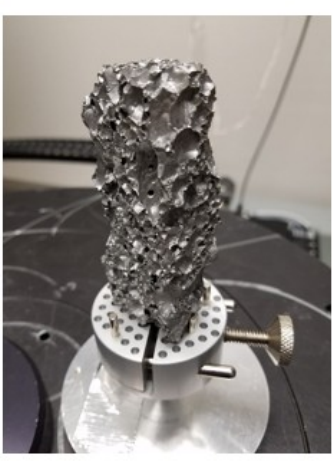




Figure 10. Early prototype version of cold CT setup at NASA GSFC (newer version uses more insulative materials). Cold immersive environmental chamber is allowed to rotate underneath fixed cryogenic feed lines. Sample shown here was a block of aluminum foam, cooled under  $N_2$  at -100 degrees C.

Once the environmental XCT scan has been captured, there are a number of interesting applications for the dataset. One obvious benefit is that the data could be very useful in failure assessment (particularly relevant for space applications), in which a part may have failed during testing at cold exposure but performs nominally at ambient. Another useful application is to make use of the differential between the environmental scan (at cold temp, for example) and ambient or other temperatures. Material coefficient of thermal expansion (CTE) would then be measurable in multiple directions, both internally and externally. One could also measure internal strains (as a result of thermally-induced stress) via advanced processing tools such as digital volume correlation (DVC, analogous to the more common digital image correlation, DIC for external surfaces). There are both commercial software tools (such as Correlated Solutions' "VIC Volume") and open source software tools for this type of analysis.

## 2.9 In-situ Mechanical Testing

Accessory stages can also be used to conduct in-situ mechanical tests and capture XCT results while the sample is under an applied load, whichcan provide insights regarding failure mechanisms. These are primarily conducted with incremental loads and static XCT scans to prevent motion artifacts that would occur if the sample was dynamically moving during the course of the scan acquisition. Polymeric samples or samples that are known to exhibit creep and stress relaxation typically have a holding step between loading and scanning to prevent motion artifacts.

## Example 1: Compression loading of polymeric trusses

Crack propagation and growth can be studied as illustrated in Figure 11 (left), which is a polymeric truss made with EnvisionTEC resin. The images at the top are at the same location of the sample as the letters indicated on the load versus displacement curve. Figure 11 (right) shows a more elastic polymeric truss structure manufactured with FormLabs Clear resin. This demonstrates the feasibility of measuring deformation and truss collapse behavior with in-situ XCT. If differing density particles of proper size and

shape are within the truss structure, then strains can be measured using VIC as mentioned briefly in the previous section. The in-situ loading can also be combined with a heating or cooling stage to study deformational changes at certain temperatures. One such study explored the micromechanical deformation of snow [33].

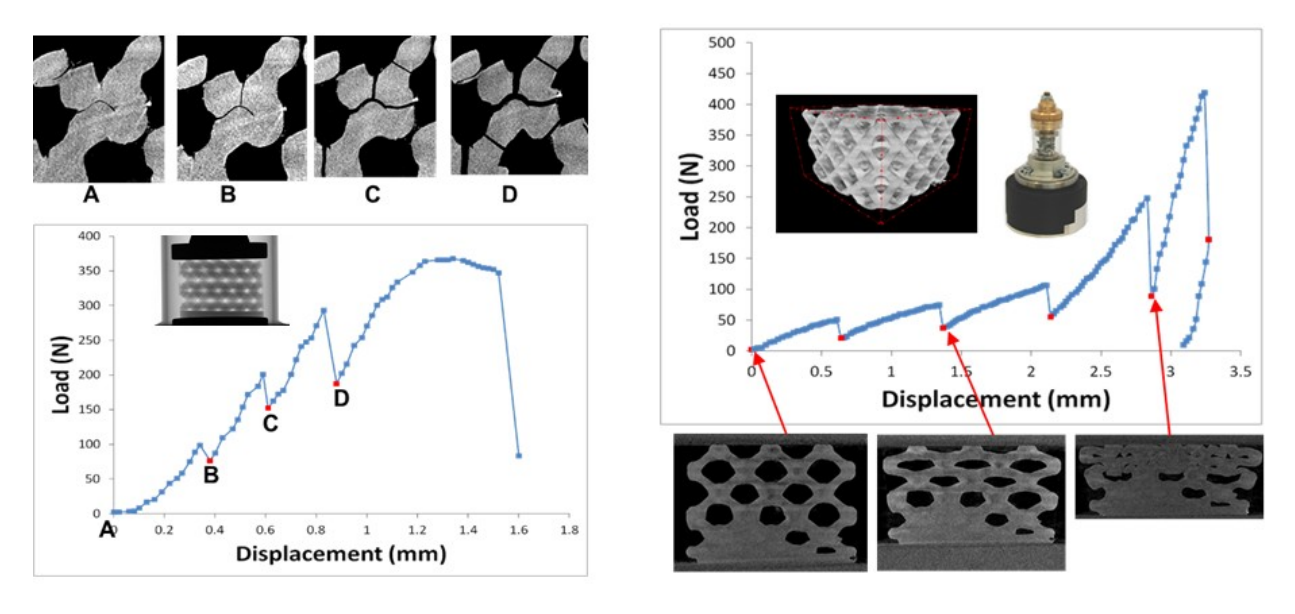


Figure 11. In-situ compression of polymeric trusses demonstrating crack propagation (left) and deformation (right)

### Example 2: Tensile loading and cavity formation

Another example is the formation of cavities during in-situ tensile loading. Figure 12A shows glass spheres that were segmented and colorized by volume and the segmented cavities are shown in red. Figure 12B-E demonstrates that the cavities formed on all sizes of glass spheres, qualitatively indicating there was not preferential formation on larger glass spheres. This technique was further used to explore the size distribution of cavities with and without an engineered coating and at varied load levels to determine the effectiveness of the coating for improved strength as well as discern the importance of the glass size distribution [34]. Advanced segmentation methods were used to isolate glass spheres that had attached cavities to directly compare to the distribution of all glass spheres and quantitatively prove the qualitative results shown in Figure 11.

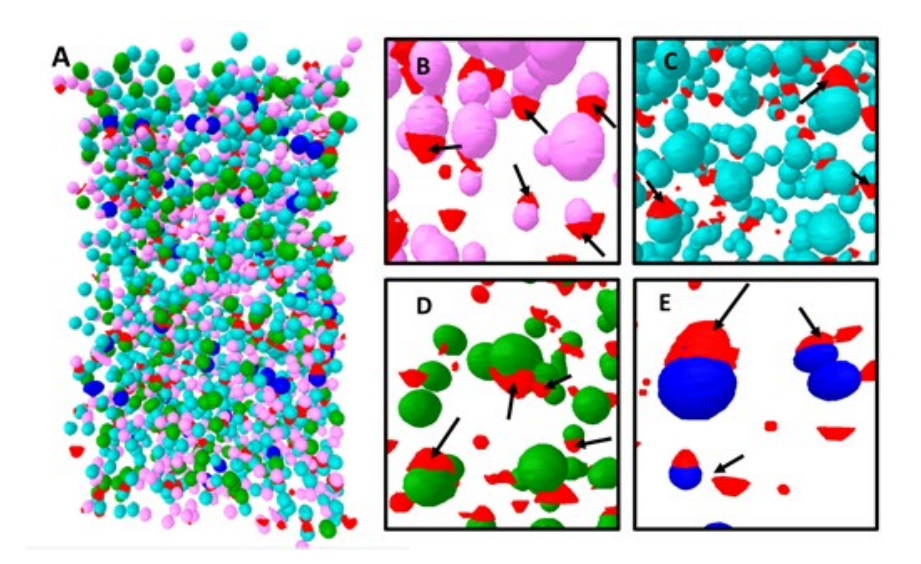


Figure 12. Segmented glass spheres by volume: 2000-4000 voxels (pink), 4000-6000 voxels (light blue), 6000-8000 voxels (green), and >8000 voxels (dark blue) and segmented cavities in red (Reproduced with permission [34])

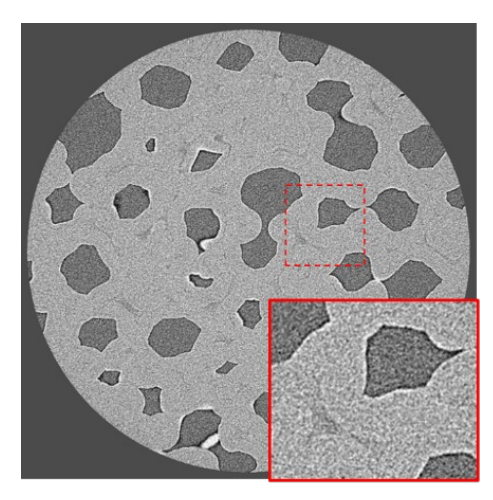
## 2.10 4D Scanning

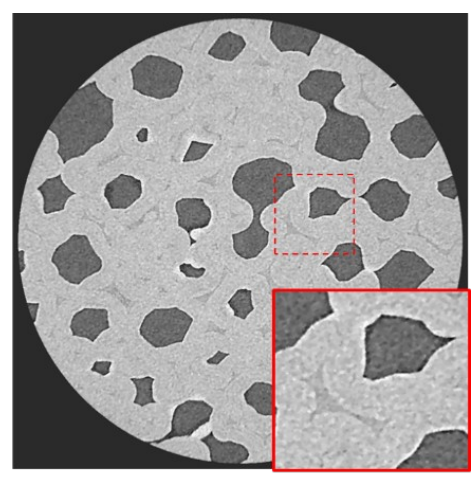
4D scanning is a process that generates dynamic 3D XCT scans, capturing motion over time. The motion can be captured either through compiling sets of subsequent static scans or dynamically if the acquisition time and sample movement timescales are compatible. The static method would apply a movement and then hold the part in that position for the entirety of the scan and that process would be repeated through the last stage of motion. These sets of scans are merged and played continuously, similar to a picture flip book in two dimensions. The dynamic method would entail slow loading speeds for in-situ mechanical testing or other slow events such as ice melting or gradual fluid flow with fast acquisition times to prevent motion artifacts. There are advantages and disadvantages to each method. The static method provides cleaner results with less noise since the scan settings can be optimized with more projections, lower energies, or higher frames averaged. The dynamic mode has a much shorter overall scan time and can capture the full range of motion rather than interpolation between static positions. Another method that has been used to capture motion in even shorter timescales is the use of multiple source and detectors across from one another that capture specific angles. This technique allows for higher speed events or slower scans that would result in higher quality results.

#### 2.11 Iterative Reconstruction

Traditional reconstruction methods mostly use a filtered back-projection process, which is typically very fast but can sometimes result in a large amount of noise in the images. An alternate method called iterative reconstruction uses a cyclical process to predict an estimated forward projection, which is then compared to the actual measured projection. Differences between the two images are taken into account to back-project an updated image. This is repeated a set number of iterations or until the differences between the two images reach a particular value. The primary advantage of using an iterative reconstruction algorithm is either improved quality of the resulting images (usually a substantial reduction in noise or in some cases improved contrast between phases) or similar quality results with a fraction of the number of projections, which can significantly reduce the overall scan time.

Figure 13 demonstrates noise reduction between the traditional reconstruction algorithms and an iterative reconstruction algorithm on a glassy carbon foam. With the standard reconstruction, there is a significant amount of resulting noise that would make the segmentation very difficult, particularly between the two different material phases. The iterative reconstruction not only reduced the noise in the post-reconstructed images, but also improved the contrast between phases which would allow for much easier segmentation and quantitative analysis.





Standard reconstruction

Iterative reconstruction

Figure 13. Iterative reconstruction example of a glassy carbon foam demonstrating a reduction in noise and improved contrast

# 3. Post-scan Analyses

The case studies in this section primarily focus on analysis techniques to achieve valuable and meaningful data from XCT scans. While 3D volume renderings and segmented visualizations are excellent ways to highlight certain phases in specific colors and emphasize particular features within a sample, quantitative data and advanced analysis techniques aid the understanding of fundamental material relationships or explain the reason for failure. In this section, many examples will be shown and they are categorized by tolerance deviation analysis, porosity analysis, fiber orientation analysis, and failure analysis.

## 3.1 Advanced segmentation

The topic of image segmentation (which may involve several filtering or image processing steps) clearly has applications beyond the confines of XCT, and therefore could not possibly be properly represented in full, so only a brief mention of some relevant applications will be presented here. Image segmentation is relevant to XCT for a number of reasons. One key benefit is in data reduction of the processed reconstructed volume (or perhaps even the raw captured images *prior* to reconstruction). For production environments, or even medical applications, specialized segmentation and filtering routines could be highly impactful for isolating material boundaries, generating clean edges of scan volumes prior to surfacing (for 3D printing, for example), and finding defects which may be obscured by scatter or image noise. One major challenge to all these routines is the ability of the algorithm to properly threshold or segment areas of the scan where there may be non-uniform gradients in image intensity, noise level, or contrast. Adaptive segmentation methods (for example Image Pro 3D Smart Segmentation) that work off of machine learning tools, teaching algorithms (using local seed points, for

example), or recursive algorithms show much promise in helping to correct for these local gradients [35]. An example using a hierarchical image segmentation is shown in Figure 14. This was a particular situation where the sample was packaged in a container that caused some scatter and reduced contrast. Of particular interest with this sample was isolating the outer surface and cleaning the internal pore walls so that volume calculations could be done. Segmentation processes such as this have potential to better isolate materials and clean borders in images/volumes that contain local shading gradients due to scatter, beam hardening, etc.

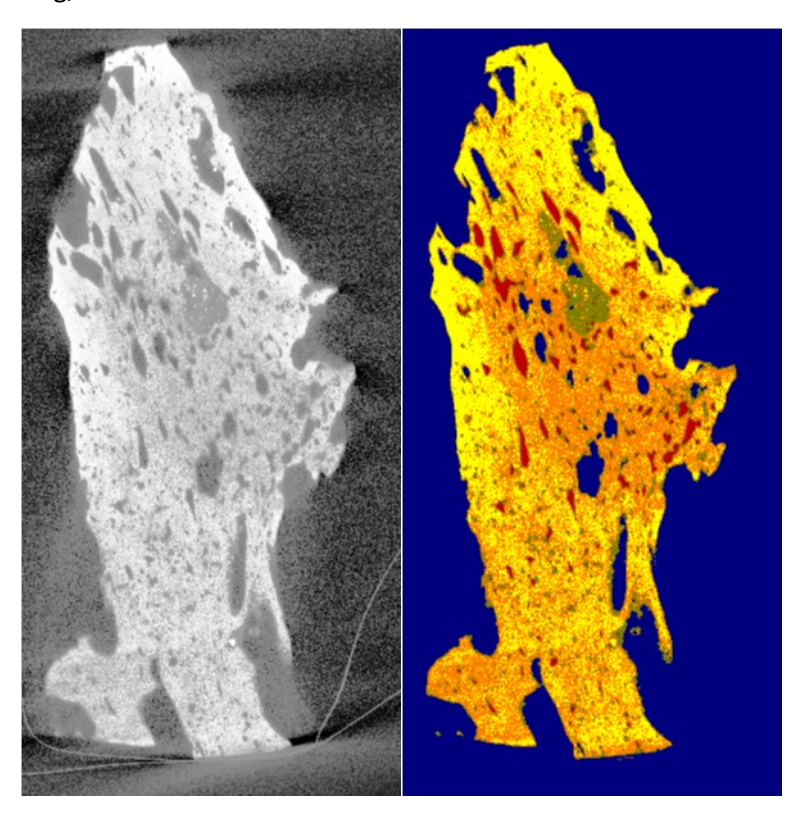


Figure 14. Recursive hierarchical image segmentation of rock glass tektite from Zhamanshin meteorite impact crater. (Segmentation tool by Tilton et al)

One highly impactful application of image segmentation is in automatic defect recognition (ADR). This is particularly relevant for production environments, or when the number of potential defects (or features of interest) is prohibitively high for manual investigation [36]. ADR tools face the same challenges described above relevant to local gradients in contrast, noise, scatter, etc., so the better tools must be capable of adapting to these local volume differences (either automatically, through machine learning sets, or via user input). Also, while not common, advanced segmentation and ADR tools have appeal for applications where data downlink is a challenge (remote field use, mining applications, space environments, etc.). The tools could be used for reducing the relevant dataset to only a fraction of the original full reconstruction. Converting a full volume with 8-, 16- or 32-bit voxels into an object class based volume, in which segmented regions of full bit depth voxels are replaced by a class identifier, would drastically reduce the file size, though obviously imposing a greater risk of throwing away subtle contrast differences that may be relevant in distinguishing certain features. A subset to this approach is the concept of removing useless voxels containing "air" volume beyond the outer surface of the part.

These voxels could be replaced by a lower bit depth value, removed altogether, or even replaced with a binary value (similar to a 2D "mask").

More advanced porosity segmentation is possible, especially if there is a large size difference between the features of interest. Figure 15, for example, shows a 3D model generation of a segmented aluminum phase and the internal voids in red, while excluding the external air. The air phases were segmented from one another after the original thresholding included both air that was external and internal to the aluminum truss structure. Only the internal porosity was of interest, so additional image processing steps such as despeckling and bitwise operations can isolate the internal voids from the external air for additional visualization and quantification.

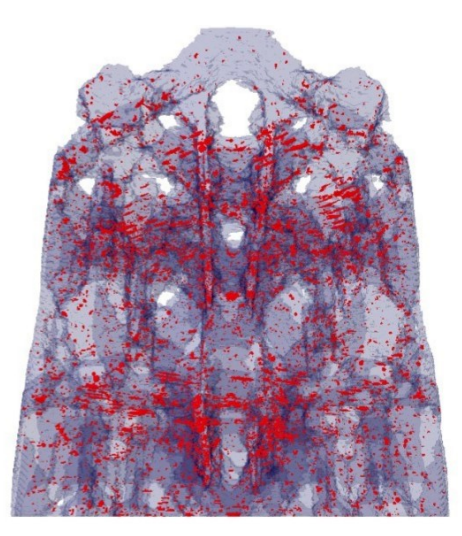


Figure 15. Internal porosity segmented from external air surrounding an aluminum truss structure

## 3.2 Tolerance deviation analysis

Dimensional metrology is important for quality control and inspection, and XCT is the only known method to be able to concurrently evaluate both internal defects and dimensional accuracy non-destructively [37]. Manufacturing metrology has also been shown to provide substantial cost savings to businesses through reducing part failures that occur during a warranty period and reducing liability due to part failures that may cause harm or injury [38]. XCT can be utilized to evaluate dimensional differences between the manufactured part and the original CAD drawing. This technique can even be implemented on a production line with automatic acceptance and rejection criteria.

Dimensional analysis is also important for life cycle assessment of a part when wear and degradation over time may lead to failure. Corrosion on a part may cause pitting or external deposits that may be problematic. XCT can be used to quantify deviations between a damaged part and a clean or untested part. This method is valuable to learn if there are specific problematic areas in a particular location of the part or if there is a tolerable degradation distance before removal from service for replacement or repair.

Other deviation analysis methods, such as laser scanning, are valuable on large parts with simple geometries. Laser scanning uses a line-of-sight technique, however, so more complex parts with internal channels, truss structures, or more advanced topologically optimized geometries are not able to be fully captured. This is becoming increasingly important due to the complexity of additively manufactured

components. XCT overcomes the line-of-sight laser scanning limitations and allows for the 3D analysis on the full geometry, including deviations of internal features.

The analysis technique involves defining the boundary of the XCT scanned part through common thresholding methods. The software used for the examples presented in this section is Volume Graphics (v 3.0) and the thresholding processes are called "surface determination". After defining the surface boundary, the XCT scan is registered to the CAD drawing (or other XCT scan if comparing two different scans). The registration process aligns the two objects so that they are in the same orientation based on matching a majority of the surface points to one another. The module called Nominal/Actual Comparison was used for the quantitative deviation analysis. First, an application of manufacturing process improvement is shown through comparing two different manufacturing methods. Next, the technique is demonstrated on a titanium bracket to measure the amount of deformation due to residual thermal stresses and the subsequent reduction after modifying the heat treatment. Lastly, the analysis is used on two different XCT scans before and after impact testing on a helmet. These examples demonstrate several different ways the analysis can be utilized for process optimization, quality control, and failure analysis applications.

# Example 1: Comparison of part deviations for different additive manufacturing methods

Polymeric additively manufactured parts are important to print near net-shape since they are not typically machined to their final dimensions [39]. Polyjet and Fused Deposition Modeling (FDM) methods were used to manufacture the same topologically optimized gear. This complex design would not be suitable for laser scanning due to the internal features and inability to measure them. The XCT scan, however, captures the full 3D volume and is directly compared to the CAD drawing. Figure 16A shows the polyjet and FDM manufactured gears in gray and the CAD drawing in blue. The tolerance deviation analysis is shown in Figure 16B with the colored bar indicating the deviation lengths above or below the target value of the CAD drawing. The histograms shown in Figure 16C quantitatively show that the polyjet manufacturing process was much more precise than the FDM process for this application at achieving the design geometry. This technique can also be used for optimizing specific process parameters to achieve improved accuracy, especially when tight tolerances are needed. Additionally, cumulative deviations within the absolute value of the target distance can readily be quantified. Ninety percent (90%) of all the deviations were within 0.207 mm for the polyjet printed gear, whereas 90% were within 0.469 mm for the FDM printed gear.

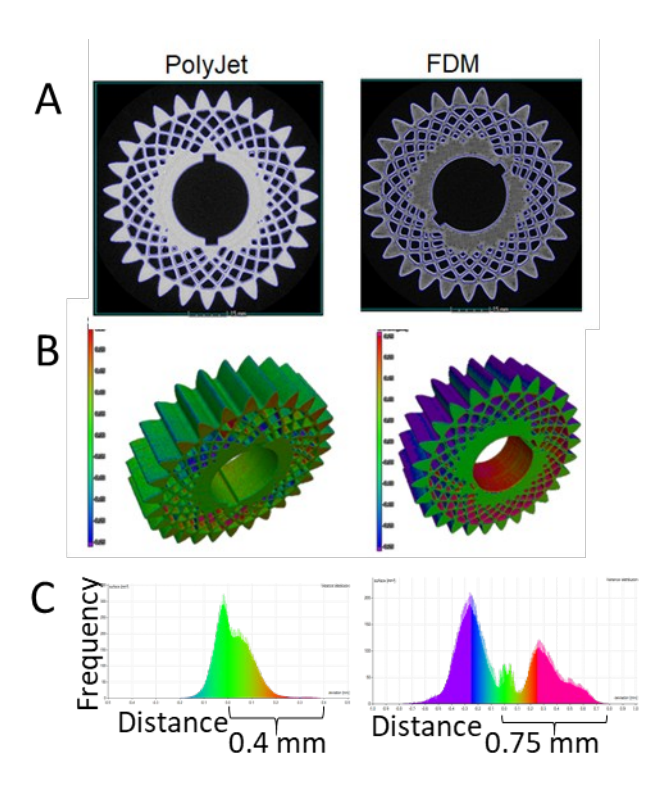


Figure 16. Deviation analysis for a topologically optimized gear manufactured by polyjet and FDM processes A) CT scans in gray and CAD drawing in blue B) deviation analysis on the 3D volume rendering and C) histogram results showing the polyjet process is closer to the design than the FDM manufacturing process

### Example 2: Quantification of deviations due to thermal residual stress

Another deviation analysis example shows improvements in the final part geometry due to heat treatment modifications to reduce thermal residual stresses. It is well known that additively manufactured parts can have large thermal residual stresses that can significantly reduce mechanical performance or lead to early part failure [40]. A direct metal laser sintering (DMLS) titanium bracket was manufactured and part of the bracket experienced large distortions on the order of 5 mm as illustrated in Figure 17B. After modifying the heat treatment, the residual stresses were reduced and the part exhibited only 1 mm distortions after being cut from the build plate (Figure 17C).

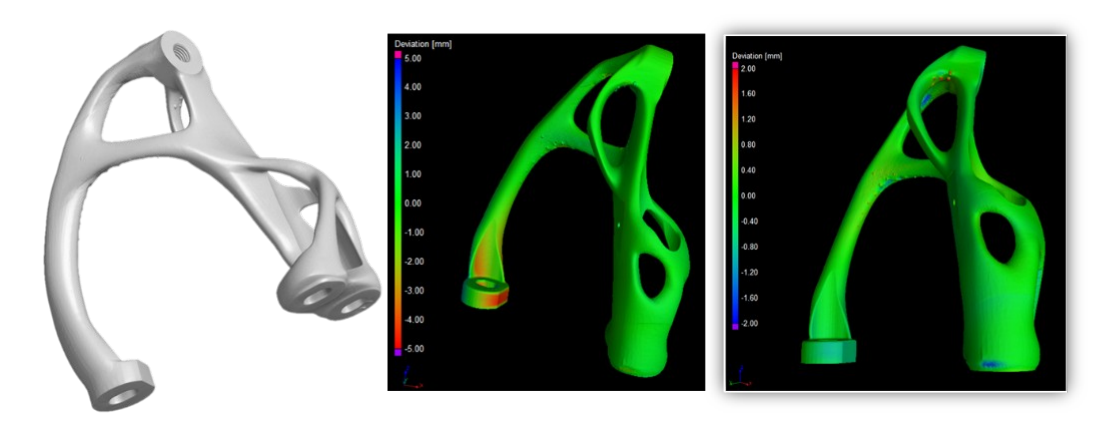


Figure 17. Additively manufactured titanium bracket A) 3D volume rendering before quantitative analysis B) with large deviations due to large thermal residual stresses and C) improved tolerance after heat treatment modification

### Example 3: Deformation quantification of a helmet after impact testing

The nominal/actual comparison analysis technique can also be used when comparing two different XCT scans rather than solely an XCT scan to an original design or drawing. An example of this is shown in Figure 18 of a helmet scanned before and after drop tower impact testing. Both the extent of deformation and delamination can be measured and the quantitative results can be linked to the forces experienced during the impact testing. This can provide valuable information for improving the accuracy of computational models as well as determining the maximum forces possible before significant deformation occurs.

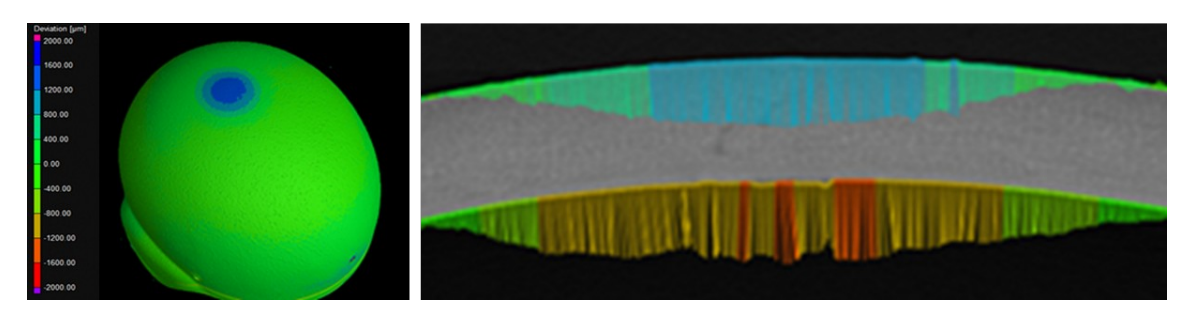


Figure 18. Helmet deformation after drop tower impact testing with the 3D volume rendering (left) and 2D cross-sectional image (right) showing deformations on the order of 2 mm

## 3.3 Porosity Analysis

Porosity quantification is a very common microstructural analysis due to the importance of reducing porosity to achieve improved performance. XCT is extremely beneficial for porosity quantification due to the ability to discern location dependencies as well as an understanding of the shape and morphology of the pores. Traditional methods such as optical microscopy are 2D and severely limit the volume analyzed as well as the information that can be gathered. XCT not only provides the full 3D volume, but porosity is often very easy to segment due to large contrast changes between the air and the bulk material. This is due to large changes in the mass attenuation coefficient, so automatic thresholding segmentation algorithms can often be successfully implemented. Common quantitative analyses with XCT porosity evaluation include overall 3D void volume percentage, porosity as a function of distance, pore sphericity, and histograms of the void volumes.

### Example 1: Reduction in porosity with improved processing

Porosity can be an important microstructural feature to reduce when optimizing a manufacturing process. Oftentimes there are numerous processing parameters that can be adjusted that have a significant impact on resulting porosity and therefore material performance. XCT can help identify critical processing parameters that minimize porosity. Fused deposition modeling (FDM) additive manufacturing involves several processing variables, such as print speed, extrusion temperature, bed temperature, and nozzle geometry. XCT was able to quickly identify that a slower print speed significantly reduced the porosity, as shown in the 3D volume renderings in Figure 19, and was more important than several other processing parameters. The samples shown in this figure were printed under identical conditions (205 °C, degrees Celcius, extrusion temperature and 60 °C bed temperature) and the only processing variable change was the print speed. The overall porosity was reduced from 2.71 to 0.31%, strictly by reducing the print speed.

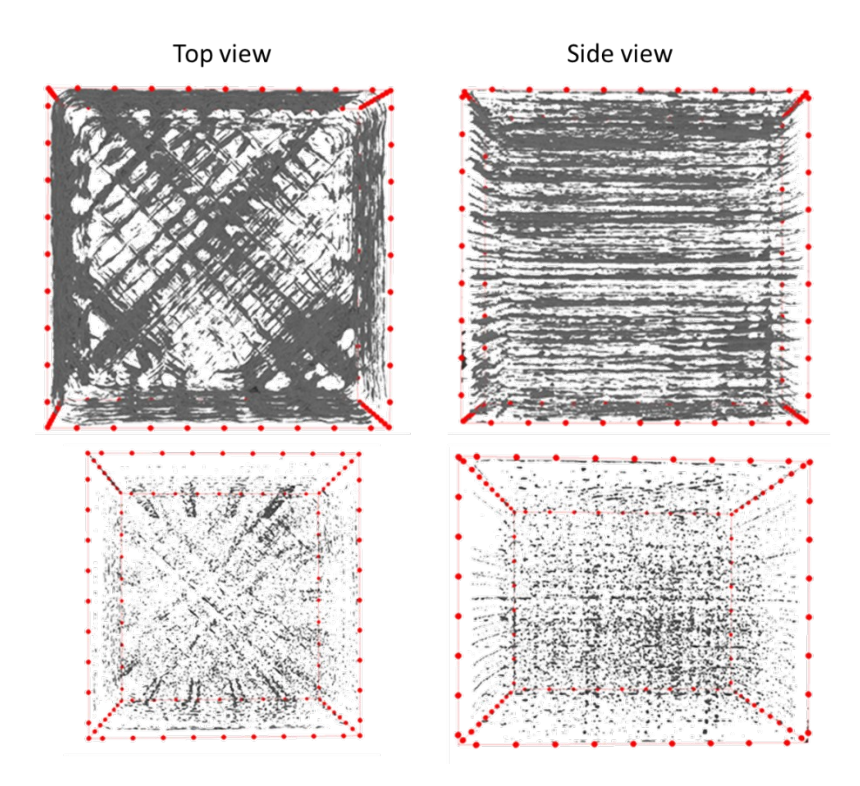


Figure 19. 3D volume renderings of isolated voids in FDM prints with a fast print speed (top row) and slow print speed (bottom row); spacing between red dots is 1 mm

Porosity was further reduced through the application of a plasma surface treatment on the filament prior to printing. 3D volume renderings are shown in Figure 20 with isolated voids from the untreated filament shown in red and isolated voids from the treated filament shown in blue. Quantitatively, the overall porosity was reduced from 0.62% using the untreated filament to 0.07% with the treated filament. The maximum void volume was 9.7 times smaller and the average void volume was 7 times lower than the untreated filament sample. Additionally, the sphericity of the voids was measured, which showed a significant difference in the shape and morphology, particularly of the larger voids. This is important for FDM parts, because linear voids are often located at the interface between fused filaments and are frequently the source of failure initiation through having a weak inter-laminar interface without a post-process thermal anneal [41]. The XCT void analysis correlated well with mechanical test data, with the untreated filament and elongated voids having much lower fracture toughness results compared to the treated filament with spherical voids.

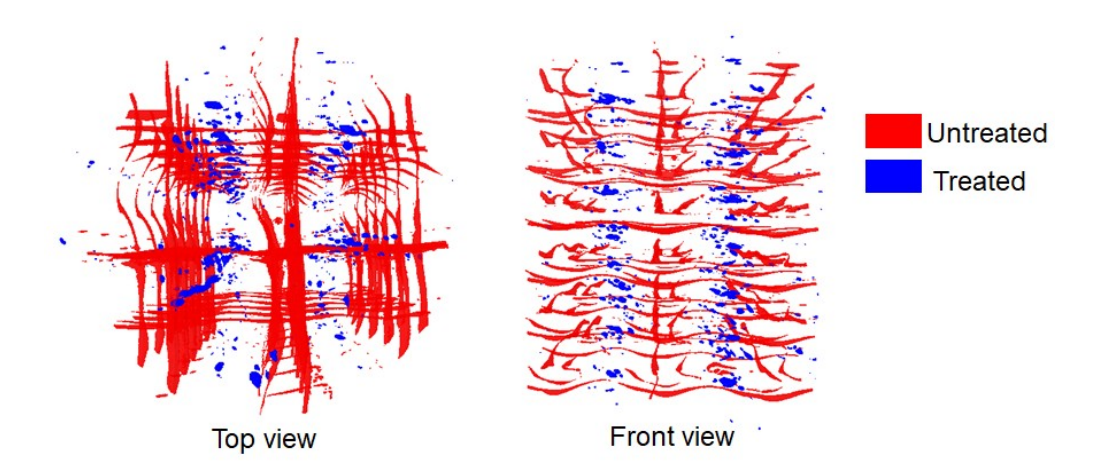


Figure 20 Void volume as a function of sphericity for treated and untreated filaments for FDM additive manufacturing demonstrates a reduction in void size as well as improved sphericity with the surface treatment

### Example 2: Understanding the relationship with mechanical performance

Aluminum trusses infiltrated with dicyclopentadiene (DCPD) resin were scanned after compression testing to explore the effects of void pockets and cracks that formed due to rapid thermal cooling. It was found that the sample with the least amount of cracking had the highest compression strength and the sample with the highest average porosity had the lowest strength. The maximum peaks within the porosity profile throughout the sample height alternated between peaks due to unfilled regions (void pockets) and peaks due to DCPD cracking. This is illustrated in Figure 21, demonstrating the microstructural changes as a function of sample height. The broader peaks are correlated to the cracking within the resin and the sharp, narrow peaks are unfilled resin regions or voids. Comparing the DCPD micro-XCT results with the compression testing results, the magnitude of resin cracking was the dominant mechanism for failure and the resulting compressive strength.

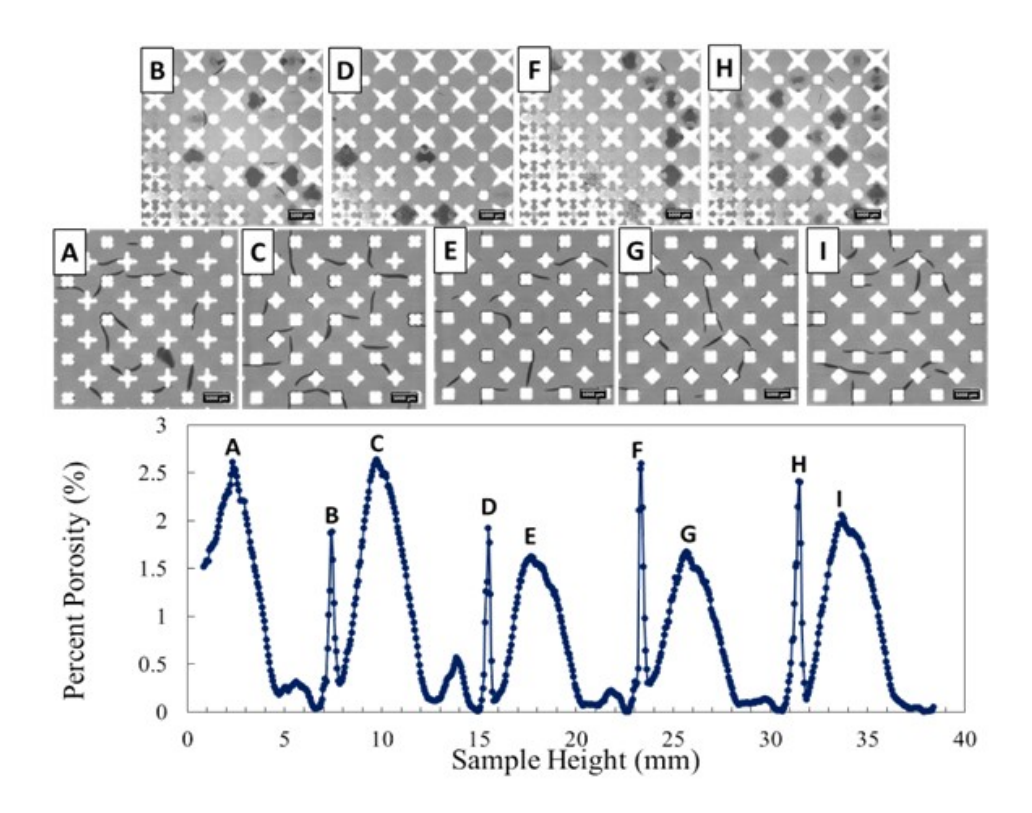


Figure 21. Porosity as a function of distance results for a DCPD infiltrated aluminum truss helped discern that the cracks formed due to rapid resin cooling (locations A, C, E, G, and I) governed the compression failure rather than the void pockets of unfilled resin (locations B, D, F, and H)

#### 3.4 Fiber orientation

It is well known that fiber orientation plays a critical role in the resulting mechanical behavior of composite materials. Several methods have previously been used to quantify fiber orientation experimentally; however, many historical techniques such as the "method of ellipses" are based on 2D images and do not capture misorientations within the full 3D composite. Considering most commercial fibers are on the order of approximately 10  $\mu$ m in diameter, obtaining adequate resolution for detectability is challenging. Fiber orientations can be captured, however, on small samples and provide orientations in the full 3D volume. CT can capture a larger volume compared to optical microscopy as well as overcome the common issue of ambiguity when it is unknown if a fiber is rotated positively or negatively in relation to the symmetry plane.

Fiber-level resolution for 3D XCT was first achieved at synchrotron facilities. Some studies involved insitu mechanical testing and quantifying the change in fiber orientations or evaluating failure mechanisms in fiber composites [42-45]. After laboratory scanners advanced to achieve higher resolutions that can detect fibers, experiments have confirmed similar results between the synchrotron and laboratory systems [46]. Several methods have been used to quantify fiber orientations, including commercial software [47-50] and custom codes [51, 52].

### Example 1. Misaligned fibers between plies

A 4-layer quasi-isotropic lay-up of +45/-45/90/0 IM7 carbon fiber with dicyclopentadiene resin was used to conduct an orientation analysis and determine if misaligned fibers could be detected. The scan voxel size was 0.75  $\mu$ m and Volume Graphics VG Studio Max v 3.0 was used to conduct the orientation

analysis in the plane projection mode. Figure 22 shows misaligned fibers were detected between the 90 degree ply (red) and the 45 degree ply (yellow). The misoriented fibers are shown in blue and are between 60 and 84 degrees. This technique successfully demonstrates the ability to detect and quantify the degree of misalignment, which can be used for processing optimization or quality control assessments.

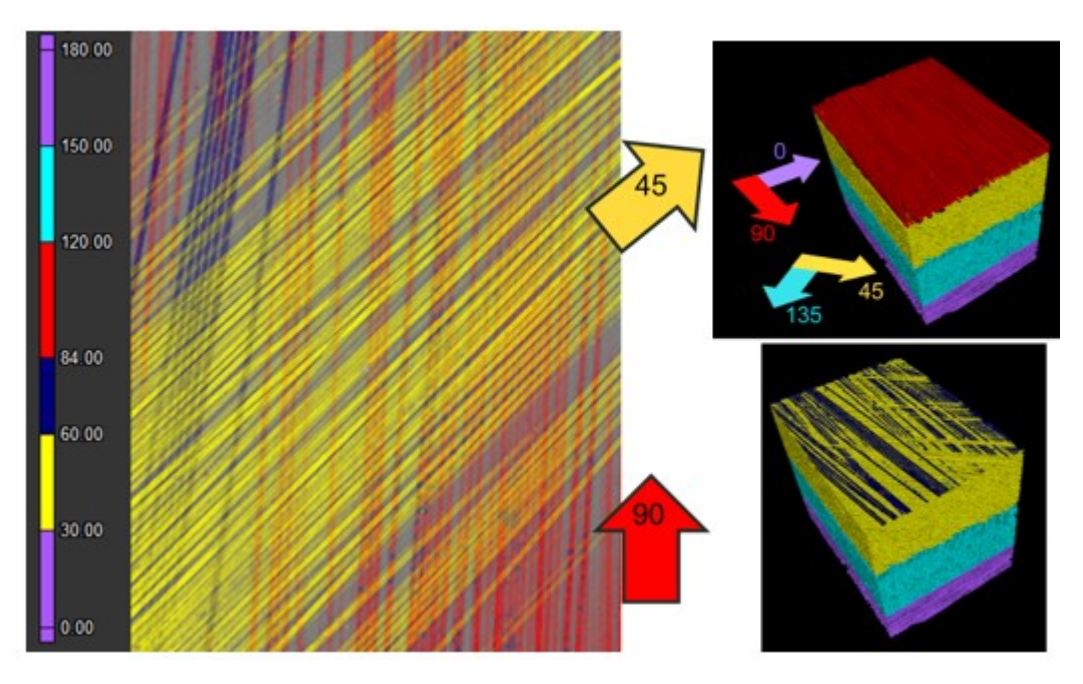


Figure 22. 0.75 μm voxel size scan demonstrated the ability to capture misaligned fibers between layers of a 4-layer quasiisotropic composite laminate. (Reprinted with permission [53].)

# Example 2. Additive manufacturing print orientation of chopped fiber filament

Short-fiber composite orientations are also important for manufacturing methods such as injection molding with flow-induced orientations, since it is well known that orientations perpendicular to the applied tensile load reduce the strength to failure. XCT analysis and fiber orientation analysis could be used to experimentally verify fiber orientations in select locations of the part relative to the predicted orientation of injection molding models. More recently, short-fiber composites are being manufactured by additive manufacturing processes such as fused filament fabrication. An example of this is shown in Figure 23, with print directions varied by 90 degrees between each layer. Figure 23A and B show 3D volume renderings of a thinly sliced top view near the interface and side view, respectively. The histogram (Figure 23C) provides a quantitative assessment for the fiber orientations.

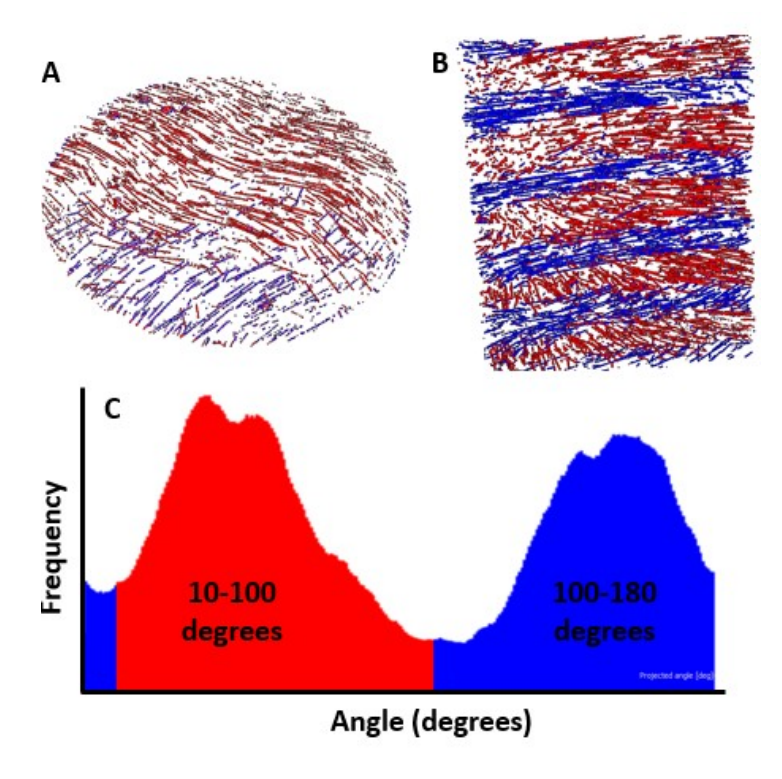


Figure 23. Additively manufactured carbon fiber filament demonstrating the predominant fiber orientation in each build layer A) top view sliced thinly near the interface between layers B) 3D volume rendering of the side view, and C) histogram response of all fiber orientations within the sample

It should be noted that in addition to fiber orientation analysis for composites, fiber volume fraction estimates can also be readily attained using similar thresholding tools as presented in the previous section. This may be used as an alternative to destructive methods such as optical microscopy (using cross-sections) or acid digestion.

# 3.5 Failure Analysis

In terms of end-use applications, one could categorize the usefulness of XCT in several ways, including quality control/verification of products, additively manufactured part inspection, biomedical applications, reverse engineering, geological sample analysis, and others. But what may be one of the most common applications, at least for engineering use of industrial XCT systems, is for failure analysis. From welds to circuit boards to composite joints and countless others, XCT has been demonstrated as a workhorse technique for particularly complex parts, or for finding hidden problems deep inside a part that otherwise would prove challenging to other NDE techniques. Provided here is a small sampling of case studies where XCT proved pivotal. Due to program sensitivities, particular details of these case studies have been omitted.

# Example 1: Circuit board failure investigation

XCT can be used for various purposes for electronics inspections, including printed circuit boards/printed wire boards (PCBs/PWBs), inspecting various components, assessing solder quality, and locating failures. There are certain limitations to the use of XCT, however, related mostly to the high aspect ratio of some boards and also to the high solder (often Pb) content of some components. XCT is not particularly good

at scanning parts that are plate-shaped, or that have a very high aspect ratio. Depending on the location or the size of the area of interest, more creative techniques such as offset scanning or partial angle scanning may be required to scan the part. Additionally, some systems incorporate an option to collect more projections at angles with the least transmission for improved results, such as Zeiss's High Aspect Ratio Tomography (HART) method.

In this particular case study, a large, populated circuit board, roughly 30  $\times$  30 cm in area, had failed during testing, but there was no visual indication of the failure site on the board and the customer did not know where the failure occurred. The large aspect ratio of the part made it particularly challenging to scan the whole part at any meaningful resolution. In this case, XCT alone was not sufficient, so additional NDE tools were used to help identify the problem. Infrared imaging was used to isolate the region of interest. The board was taken to an electro-static discharge (ESD) protected work area and then energized. Within a few seconds, a small region less than 1 cm<sup>2</sup> was retaining excess heat and glowing in the infrared. This region of the board was in itself highly populated with internal traces and vias, but it at least minimized the area of interest for more focused inspection. This was then followed up with 3D surface/optical inspection to look for any apparent anomalies and nothing was detected. The surface topography (through extended depth of field imaging) also showed no surface bulging. XCT was then used to scan that general region and it revealed an anomalous feature several layers deep within the PCB and isolated to that one cluster of circuit vias as shown in Figure 24. Another higher magnification XCT scan could then be focused solely on this region for better clarity, revealing a ruptured region of the Cu ground plane, indicative of a nearby failure, short, or arc between planes. Subsequent destructive analysis helped to diagnose the actual cause, but these would not have been possible without the XCT data which pinpointed the exact failure site.

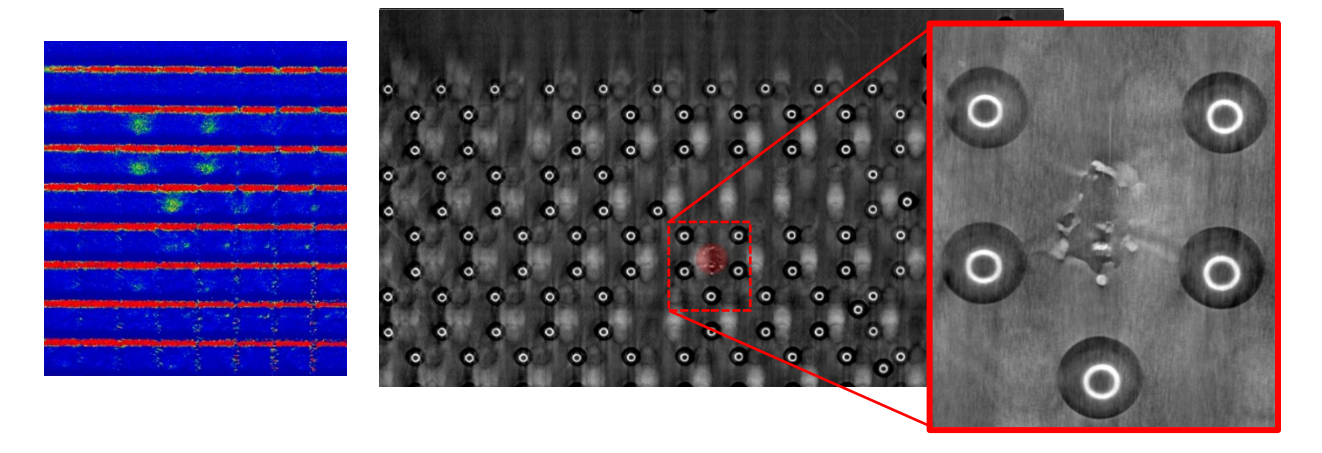


Figure 24. Circuit board NDE for failure analysis. Left image shows passive infrared image of energized PCB (only small portion of full board shown). Heated regions of the board indicated local resistive heating and potential defective region. Center image shows CT scan slice image of that section of the board and neighboring region, which showed anomalous features within the board on a particular layer. Right image shows higher magnification XCT scan slice image showing a rupture of the Cu ground plane.

### Example 2: Crack in AM Part

Here is a case study in which routine visual inspection of a part missed a critical flaw. This part was a metal additively manufactured flow device. It was actually a prototype part being used to test the efficacy of using AM as a production method. The part in question was inspected by the 3D print vendor, then inspected again upon receipt by the customer and all seemed well; however, further testing

suggested that something was wrong with the device. It was then requested to perform XCT for a more thorough inspection. The XCT inspection revealed a clearly defined crack that breaks the surface as shown in Figure 25. This crack occurred during fabrication—likely a stress relief crack. Through visual inspection of the surface, even with the knowledge of the location of the crack, this crack is completely hidden from view both to the eye and also under microscope due to the inherent surface roughness from fabrication. Without the XCT inspection, cracks like these could easily be missed. While other NDE approaches may have also found the crack, XCT was uniquely able to find the crack, render images of it in all directions, and also help verify other aspects of the part such as dimensional accuracy, porosity content, etc. While this particular part was easy for XCT due to its cylindrical geometry, it does highlight the important role that XCT plays, and will play, as various industries move toward infusing AM production methods. This is particularly true for highly complex geometries. For example, if this sort of crack was present on the interior of a complex designed part, then XCT may have been the only NDE inspection method that could have found it.

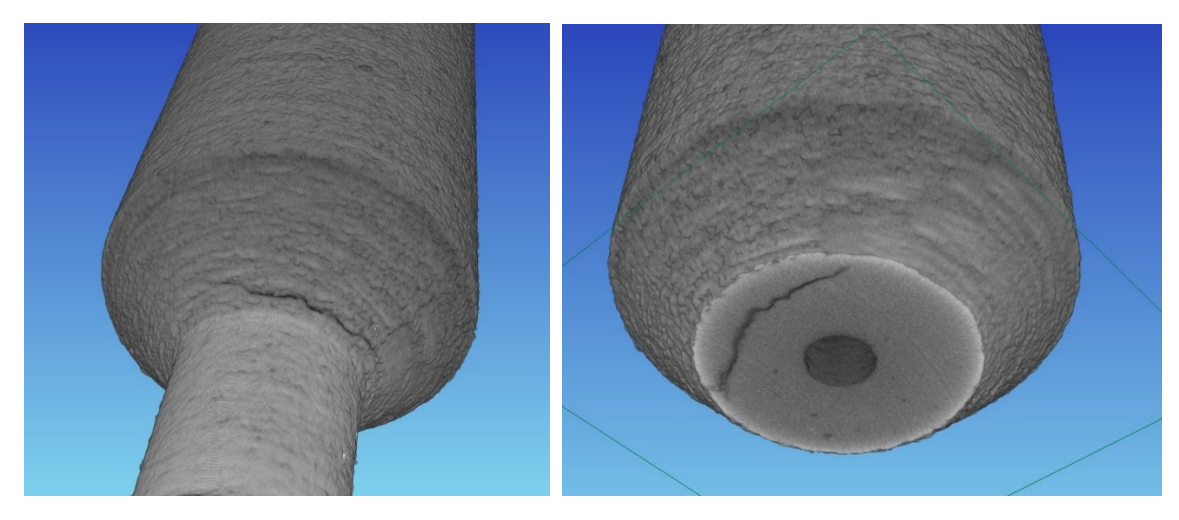


Figure 25. AM flow device with clearly defined crack that breaks the surface. This crack occurred during fabrication—likely stress relief. From the surface, this crack is completely hidden from view both to the eye and also under microscope due to the inherent surface roughness from fabrication.

## Example 3: Boroscope camera failure

During preliminary testing of a custom-engineered articulating boroscope camera, the unit failed, and all video signal was lost. For the test operators, no other indication or cause of failure could be determined, as the incoming power feed was stable, and all other diagnostic tools were functioning. This camera was intended for remote field work under extreme conditions and had remote command/control with high degrees of articulation. Several diagnostic tests were performed on the unit to assess the issue, but no determination was made. Finally, XCT was performed on the imaging head unit and cabling. The XCT inspection revealed a clear break in two of the primary signal wires that led to the sensor array as shown in Figure 26. Further investigation of the wires (away from the break) and the potting material revealed that there was not sufficient strain relief for the wires to account for the desired motion. As this was being designed as a remote sensing camera with several degrees of articulation, there was not sufficient slack in the leads nor sufficient strain relief in the jacketing to protect the circuitry on the inside. XCT was easily able to help deduce the cause of this failure, which helped immensely in the redesign of the camera.

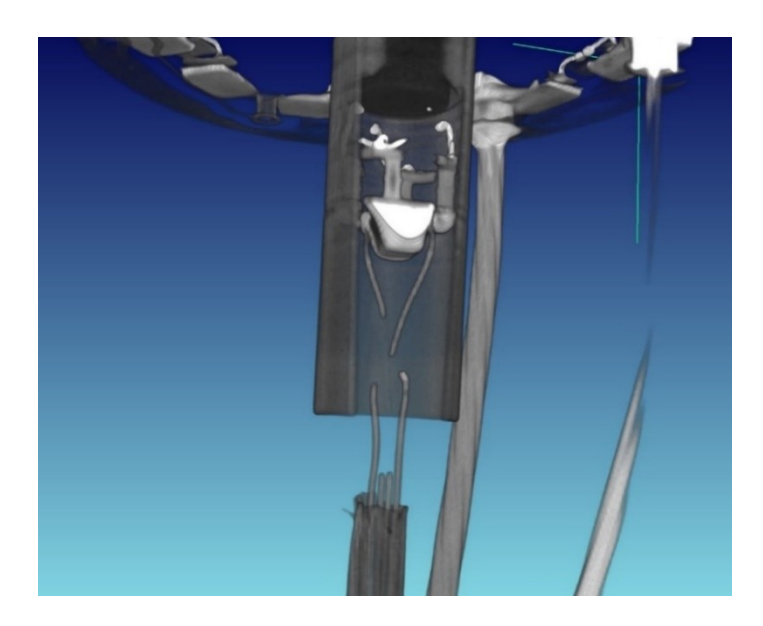
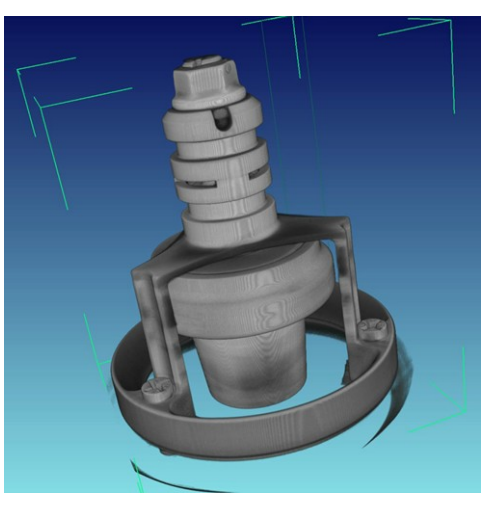


Figure 26. Borescope camera unit with broken wire leads. These wires failed during routine testing and failure was due to overstress of the articulation mechanism. Without proper strain relief to protect the internal wiring, these leads were overstressed and failed.

### Example 4: Astronaut Helmet Mishap Investigation

One particularly high visibility case study involved an astronaut aboard the International Space Station (ISS) on July 16, 2013. Astronaut Luca Parmitano was roughly 44 minutes into Extravehicular Activity (EVA) 23 when water began to enter the helmet of his space suit, obscuring his vision and impairing his ability to breathe. He was able to make it back to the safety of the ISS by following his umbilical tether. Approximately 1.5–2 liters of water eventually made it through the vent loop and into the helmet before he made it back to safety inside the ISS. NASA immediately deemed this a High Visibility Close Call and formulated a Mishap Investigation Board to figure out what went wrong and recommend measures to prevent future close calls. As part of the investigation, the team needed to understand the cause of the suit malfunction. The Extravehicular Mobility Unit (EMU) suit was returned to Earth on the next Soyuz spacecraft and then routed to labs in the US. The preliminary analysis focused the area of interest to the fan/pump/separator device in the EMU. This device was metallic and slightly larger than a softball, containing several sections and internal components. A complete teardown was planned; however, there was strong concern that physical dissection might disturb the evidence. A combination of X-ray and neutron CT was performed to non-destructively examine the fan/pump/separator, particularly the pitot tube and drum assembly. XCT successfully revealed several small contaminants that were blocking the fan/pump/separator drum holes and causing a blockage as shown in Figure 27. These were later determined to be inorganic particles. Neutron, or "N-ray" CT was a useful complement to the XCT data as it is highly sensitive to certain materials such as non-metallics (e.g., water, rubbers, grease, etc.) but not particularly impacted by metal. Though much lower resolution than the X-ray, the n-ray CT data was of higher contrast and therefore helped to confirm the contaminants and their locations and make sure no other particles were missed. Identifying these contaminants and their precise location was helpful to the MIB team in understanding the cause of the incident and aiding the next phases of the investigation.





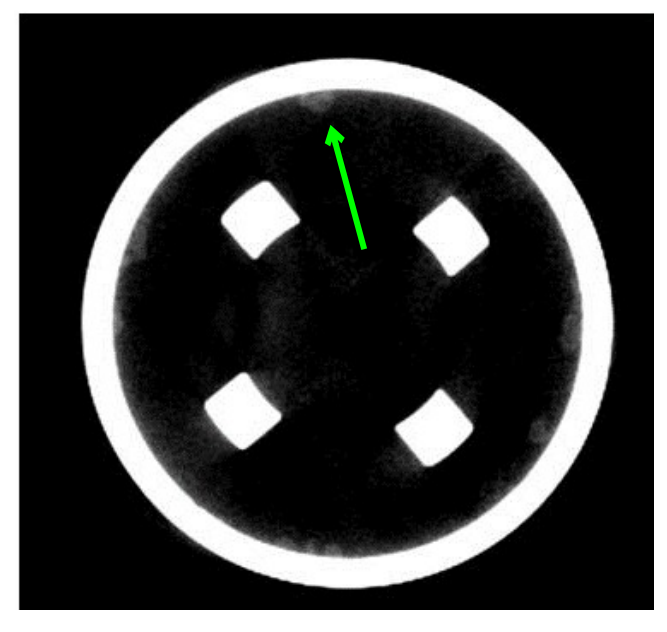


Figure 27. International Space Station (ISS) Extravehicular Activity (EVA) 23 Suit Water Intrusion High Visibility Close Call (HVCC) Mishap Investigation. X-ray CT was used to aid the investigation by discovering contamination in the drum of the pitot tube assembly of the Extravehicular Mobility Unit (EMU)'s fan/pump/separator. Because of the relatively very low absorption of the inorganic contaminant, there was very poor contrast sensitivity in the XCT images. To this end, neutron CT was also performed in conjunction to help confirm the material and locations.

# 4. XCT Practical Limitations

Sections 2 and 3 highlighted advanced scanning techniques and case studies for materials science applications and analyses. It is important to note some of the limitations, however, to understand what is practically feasible, overcome potential barriers through the modification of the sample size or selecting the appropriate scan settings, and minimizing or eliminating scanning artifacts. This section discusses one of the most common concerns for XCT scanning, which is the achievable resolution. Another common barrier for high density materials in particular is obtaining adequate X-ray transmission through the sample to reach the detector. Noise is not necessarily an XCT limitation, but can be quite problematic at times, especially for accurate segmentation for quantitative analyses. Lastly, a section on common scanning artifacts includes a description of what they are, potential causes, and methods to minimize them. Recognizing scanning artifacts is important so results will be interpreted correctly without false statements about the material microstructure that are not inherently there.

# 4.1 Spatial resolution, field of view, and geometric unsharpness

In most XCT scanners, the resulting voxel size is the field of view divided by the number of pixels across the detector. Therefore, the sample size strongly limits the achievable resolution if scanning the entire part is important. Interior tomography scans are conducted on a smaller volume inside the sample without cutting down the sample and having portions of the material extend outside the field of view.

This is not as efficient as scanning a smaller sample due to the absorption of X-rays traveling through the excess material of the sample thereby reducing the signal intensity, but it is an option to achieve higher resolution results without cutting the sample down. Secondly, unequal levels of attenuation through excess material of the sample along different X-ray paths may be reflected in the reconstructed image data and not necessarily completely representative of the scanned interior portion. Another common option is an offset scan, where two scans are conducted on each side of the sample and then stitched together.

The scan voxel size is not the true spatial resolution. Typically, features of interest require at least 3–5 pixels across them for detectability [54]. This is in part because a voxel, which is the smallest indivisible volume that can be assigned a gray level intensity, does not provide spatial contrast in and of itself; it must have gray level contrast with at least one other voxel to detect a spatial difference. Other references cite a more conservative value that up to 10 pixels may be needed across a feature for detectability [15, 16]. Therefore, if fiber level resolution is desired for a composite analysis and the fiber diameter is 10  $\mu$ m, then 2–3  $\mu$ m would be the maximum voxel size. If the scanner being used has 1024 pixels across the detector, then the ideal sample size would be approximately 2–3 mm. These relationships can often be used to assess scan feasibility and what sample size is needed in order to detect the features of a particular size.

Most XCT scanners rely on geometric magnification to improve spatial resolution, so the farther the detector is away from the sample the higher the magnification is and the lower the effective voxel size will be. There are some challenges with increasing the sample to detector distance. The simplest way is to move the detector farther away (keeping sample to source distance fixed), but this also changes the total path length for the X-rays which, due to the inverse square law, reduces signal intensity (thereby worsening the signal-to-noise ratio) and increases the geometric unsharpness. Increasing geometric unsharpness results in more blurry edges. The alternative strategy is to keep the detector and source positions fixed but increase magnification by moving the sample stage as close as possible to the source, but this runs into limitations due to sample size and also the geometric outer limits of the cone beam envelope.

The signal intensity for a point X-ray source follows the inverse square law, so doubling the distance between the source and the detector reduces the signal intensity by a factor of four. The impacts of this increased distance can be significant as the lower intensity is compensated for by increased exposure time per every single projection taken over the course of the scan. An increase of one second in exposure time to 4 or 5 seconds adds a substantial amount of time, considering thousands of projection images are taken as the sample rotates.

Geometric unsharpness is the focal spot size, F, divided by the ratio of the sample to detector distance over the source to sample distance, and is illustrated in Figure 28. It can also be written as the product of the focal spot size times the geometric magnification (M) factor minus one, or F x (M - 1), which essentially relates unsharpness to a constant for a given conventional X-ray tube (microfocus tubes typically have variable spot sizes dependent on power) and a quantity that is achievable by a variety of configurations. The focal spot size generally increases with increasing tube power, so the lowest power that provides adequate transmission is more desirable. A large geometric unsharpness results in blurrier edges and should be balanced with the scan resolution. The resolution is frequently prioritized over the geometric unsharpness and a simple calculation of the unsharpness can often show that it is dominating

over the resolution with regards to impacting the resulting image quality. In order to minimize the negative impacts of geometric unsharpness, the factor should ideally be less than or equal to one pixel.

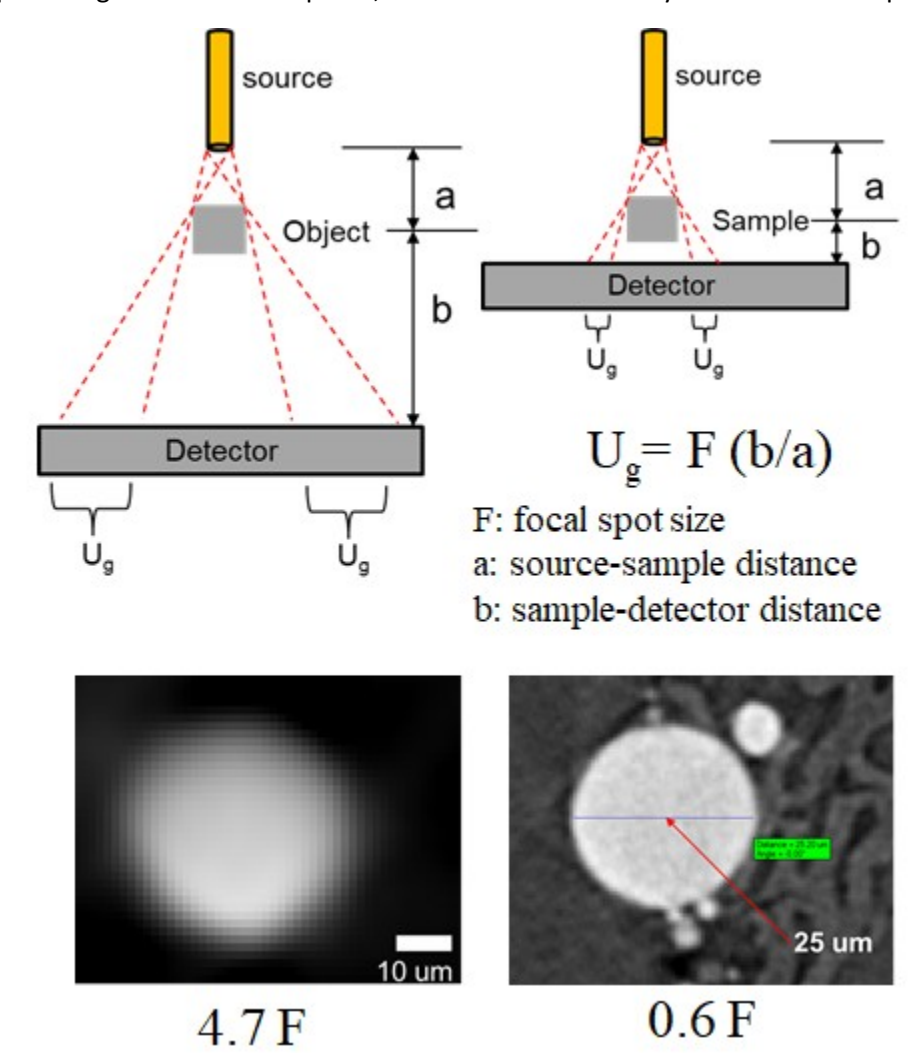


Figure 28. Illustration of geometric unsharpness (top) and example of a large and small geometric unsharpness on a titanium particle demonstrating the reduction of blurry edges with low geometric unsharpness

To demonstrate that a smaller voxel size and higher resolution is not always better, a scan was intentionally conducted with the lowest achievable voxel size (resulting in a high geometric unsharpness) as well as the minimum voxel size that had a geometric unsharpness close to one pixel. As shown in Figure 29, the voxel size of the aluminum bracket image shown on the left is about a third of that on the right image, but the geometric unsharpness is five times larger. The large geometric unsharpness is problematic for accurate edge detection as it is dominating the resulting image quality over the resolution. This demonstrates that higher resolution is not always better and must be balanced with other factors, particularly the geometric unsharpness.

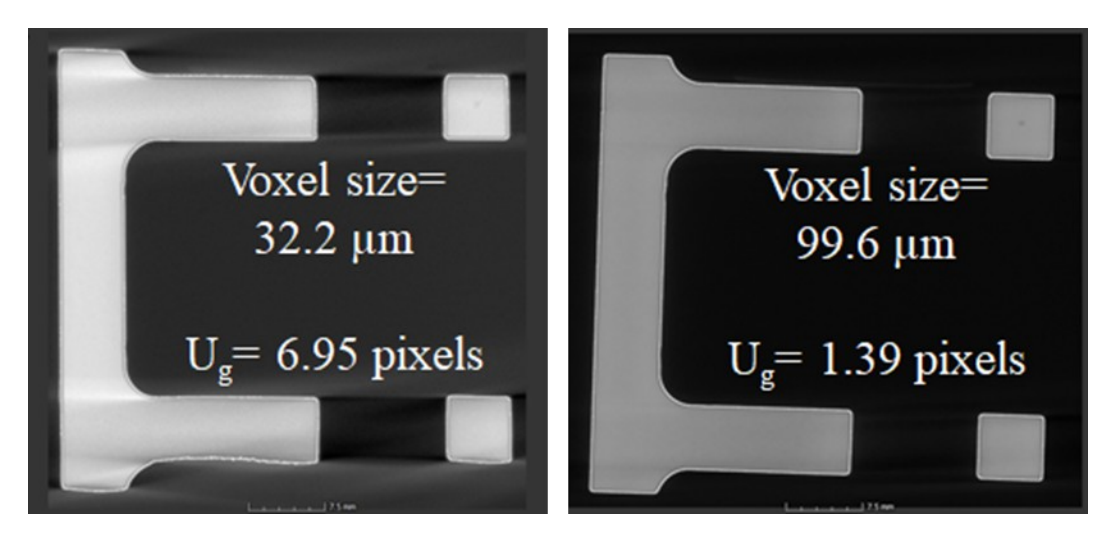


Figure 29. Aluminum bracket scanned with a low voxel size and high geometric unsharpness (left) and a higher voxel size and low geometric unsharpness (right)

XCT scanners that have objective lenses for additional magnification do not strictly rely on the geometric magnification for smaller voxel sizes and can overcome some of the geometric unsharpness limitations. This allows the detector to be kept close to the sample, reducing the geometric unsharpness and improving the signal-to-noise ratio.

### 4.1.1 Image quality indicators and representative quality indicators

When assessing the overall quality of an XCT scan, or of an XCT system (i.e., if comparing one XCT system performance to another), there are various approaches. In essence one needs to express the quality not only using resolution, but also in terms of some measure of contrast sensitivity. Here, one uses various forms of either Image Quality Indicators (IQIs) or Representative Quality Indicators (RQIs). The difference is that an IQI is a more general, calibrated tool used for some performance metric assessment of the system performance under nominal settings, whereas an RQI is a specific calibration standard which has particular similarities to the intended scan object itself.

The IQI has taken various forms for XCT systems over recent years, most of which have some series or pattern of holes, rings, wire features, etc. In the medical XCT world, these are often called "phantoms" and contain inserts with different densities to help demonstrate the sensitivity and are also used for calibration of the gray scale values to real life materials. IQIs for industrial XCT are usually intended to provide some measure of real-world resolution, aside from the nominal voxel size. One analog to the XCT system IQI is the traditional line pair gauge used for 2D radiography. While these may also be used for XCT, they are not ideal since they are typically a flat plate with information only in one plane. Another possible purpose of the IQI is to measure contrast sensitivity. This may be important because while there may be sufficient voxel resolution to identify a feature of interest, there may not be enough gray level latitude, or range, to distinguish the value of one pixel versus another. Contrast sensitivity is the measure of that ability to discern various shades of gray, and there are numerous approaches for doing so. Simply put, an effective contrast sensitivity measure is one which shows the system can detect a relevant void (in both shape and size), with similar material and thickness, under similar settings (magnification, beam power, filtering, etc.). Similar to the analog of the line pair gauge for measuring 2D radiography resolution, the plaque penetrameter is a common analog for contrast sensitivity. The penetrameter approach is to use shims of a given thickness with drilled holes in them in a size corresponding to the minimum detectable defect size. These are commonly affixed to the part and if particular holes are visible in the radiograph, then it is said to have the sensitivity needed for the inspection (in this case the sensitivity is both a function of resolution and contrast sensitivity). The problem with the traditional plaque penetrameter IQI is that they are typically flat plate-shaped objects and their 2D representation does not necessarily translate to a reconstructed image taken from multiple projection angles. A more useful representation would be a 3D IQI, made using a representative material, with some system of holes, channels, or features distributed at different locations. It also helps for the IQI to have different thicknesses, or perhaps sets of rings of different thicknesses. A common approach is a "wedding cake" structure or some sort of pyramid consisting of a thicker base layer with progressively smaller diameter levels as shown in Figure 30, with embedded features throughout. This could either be one solid part, or better yet, a nested group of parts that could be disassembled to serve as an IQI representing smaller parts (i.e., suitable for higher magnification scans, close to the X-ray source).

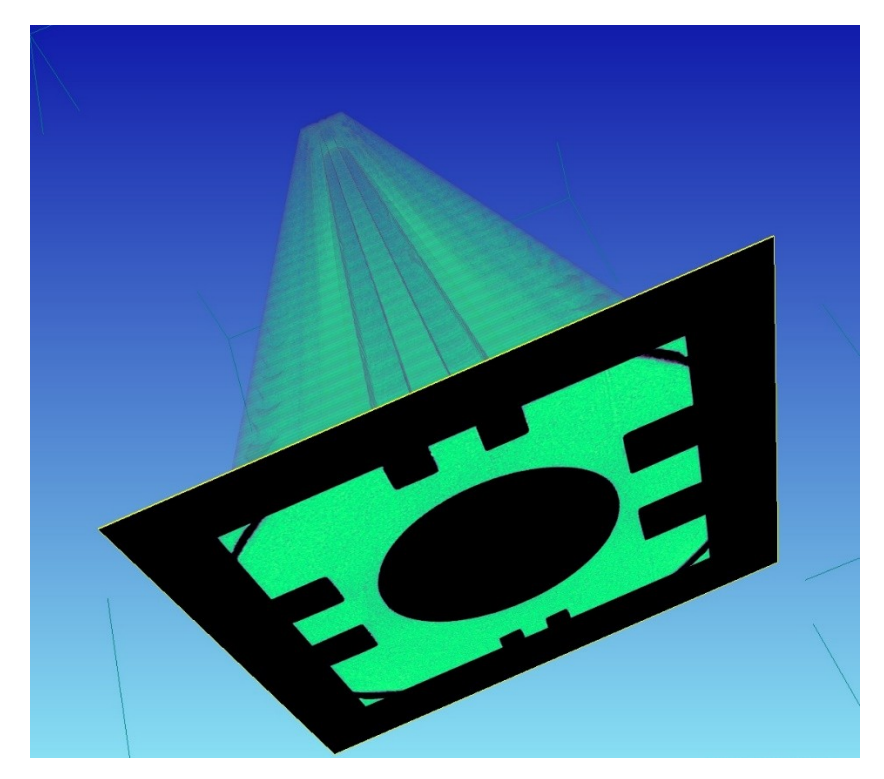


Figure 30. NASA Pyramid Image Quality Indicator (IQI) for X-ray computed tomography (US patent # 11170500). Surfaces include various sizes of line pair gauges that narrow toward the tip of the pyramid. In addition, disc-shaped penetrameters (not shown) may be inserted into center section.

The RQI may be similar in nature to the IQI in intent and implementation, but the difference is that it is considered to be more specific to the actual object intended to be scanned. It is also intended to demonstrate capability for the specific scan requirements of the inspection. For example, it may show that a crack of a certain size, in a certain location, in a particularly shaped part can be found. Take for instance a complex shaped metal 3D printed part and a customer needs to know whether the part is free of stress relief cracking of a certain size, or free of voids of a certain size. In this case, using the prototypical metal wedding cake IQI with seeded defects may not represent the nature, shape, or

location of the cracks or voids in the part. Here, the RQI should be made using the same 3D print process and with seeded defects of relevant size. These defects may be formed by various processes which are beyond the scope of this chapter, but may be artificial (e.g., programmed during the build process or post-machined, such as Electrical Discharge Machining [EDM] notches) or they may be actual defects (e.g., induced by intentionally altering a process control variable during printing or perhaps by growing cyclic fatigue cracks on the sample). Another example may be if one is scanning a PCB and inspecting for insufficient solder under a column grid array (CGA). A proper RQI in this case may be a PCB coupon made up with a mock CGA in which some posts are soldered, some are partially soldered, and some are not soldered at all. If scanning composite materials, such as end fittings on a composite tube or potted inserts, the RQI may take the form of a similar shaped composite coupon that has intentionally voided areas, perhaps created by using metal shims that are removed post bonding to create air gaps under a fitting. In whatever case, the idea is that the RQI should be as close as possible to the size, shape, material and defect of interest for the part being scanned.

### 4.2 Influences on X-ray attenuation

It is evident from the Beer-Lambert Law that X-ray transmission, the inverse of absorption or attenuation, exponentially decreases with increasing material thickness and linear attenuation coefficient. When X-rays pass through matter they are mainly absorbed by three predominant interactions: the photoelectric effect, Compton scattering, and electron-positron pair production, each occurring to varying degrees depending on the incident X-ray energy. In general, the photoelectric effect dominates at lower X-ray energies and is highly dependent on atomic number, Compton scattering dominates at higher X-ray energies, and pair production cannot occur until the X-ray energy is at least 1.02 Mega-electron Volts (MeV). The transition energy between the photoelectric effect dominating Compton scattering and the reverse of this is dependent on atomic number, and generally increases with higher atomic number [7]. The linear attenuation coefficient with units of inverse distance (cm<sup>-1</sup>) accounts for all three interactions and is dependent on both material atomic number and X-ray energy. It should be stated that the linear attenuation coefficient, which XCT image reconstruction solves for and maps, has an energy dependence that is a function of material atomic composition. This feature of the attenuation coefficient may or may not (depending on the materials and the energies of the X-rays involved) be more important than the basic density dependence. In general, the energy dependent atomic composition aspect of the attenuation coefficient is not an issue in commercial and industrial XCT scanning. In a limited number of scanning scenarios the energy dependence on atomic composition can have discernible effects over density dependence, which can sometimes be taken advantage of to improve contrast between phases. The linear attenuation coefficient can be written as the product of the mass attenuation coefficient,  $\sigma$ , typically in units of cm<sup>2</sup>/g, and the mass density,  $\rho$  (g/cm<sup>3</sup>). The mass attenuation coefficient is generally what is given in tables, along with the atomic cross section (Barns or 10<sup>-28</sup> m²), since it is independent of the density of the material and is easily calculated from the overall, or net, atomic cross section using atomic weight and Avogadro's number (N<sub>A</sub>).

Thus, net X-ray transmission through any material is dependent on a number of factors, including X-ray energy, material atomic composition and density, and material thickness. This is generally why several inches of very lightweight polymers, plastics, and polymer composites can be penetrated by X-rays, while ceramics, mixed composites, and especially metals and metal composites are much less penetrable. A simple concept used in radiography, digital or otherwise, is half-value layers (HVLs), which is the thickness of a given material that an X-ray beam of a given energy must pass through in order to

remove half of the incident X-ray intensity on the material. Thus,  $I/I_0$  is equal to 0.50. For the purpose of discussion, the linear attenuation coefficients, or mass attenuation coefficients and densities, of carbon and iron will be used for a carbon-based hydrocarbon polymer and low carbon, high iron content carbon steel with low concentrations of other elements or impurities, respectively. Using linear attenuation coefficients of 0.212 cm<sup>-1</sup> and 0.740 cm<sup>-1</sup> for carbon ( $\sigma$ =0.0953 cm<sup>2</sup>/g,  $\rho$ =2.22 g/cm<sup>3</sup>) and iron ( $\sigma$ =0.0940 cm<sup>2</sup>/g,  $\rho$ =7.87 g/cm<sup>3</sup>) at 400 keV [7], respectively, yields HVL thicknesses of 3.27 cm (1.29 inches) and 0.937 cm (0.369 inches), respectively. After X-rays have passed through three HVL thicknesses their remaining intensity is 12.5% of the original intensity, since (0.5)<sup>3</sup> is .125. A rule of thumb commonly used by industry is to keep the transmitted intensity as measured at the detector at or above about 10%. Comparing the calculations above shows that about 9.81 cm (3.86 inches) of relatively lightweight, low density hydrocarbon polymer material can be penetrated by 400 keV X-rays before losing too much intensity, while only about 2.81 cm (1.11 inches) of low carbon, high iron content steel can be penetrated, exemplifying the stark difference between these types of materials.

The influence of varied X-ray voltages and material thickness is demonstrated in Figure 31. Aluminum rods ranging in size from 1 to 3 mm in diameter were imaged at voltages ranging from 40 to 160 kV (maximum X-ray energies ranging from 40 keV to 160 keV) in increments of 20 kV (energy increment of 20 keV). Transmission percentages were obtained after taking a background image and applying that reference image to the captured digital radiograph. Line profiles were drawn across the images giving the results shown in Figure 31, which demonstrates the expected trends that larger diameter samples have less transmission at the same voltage or energy and that higher energies have more transmission for the same sample size.

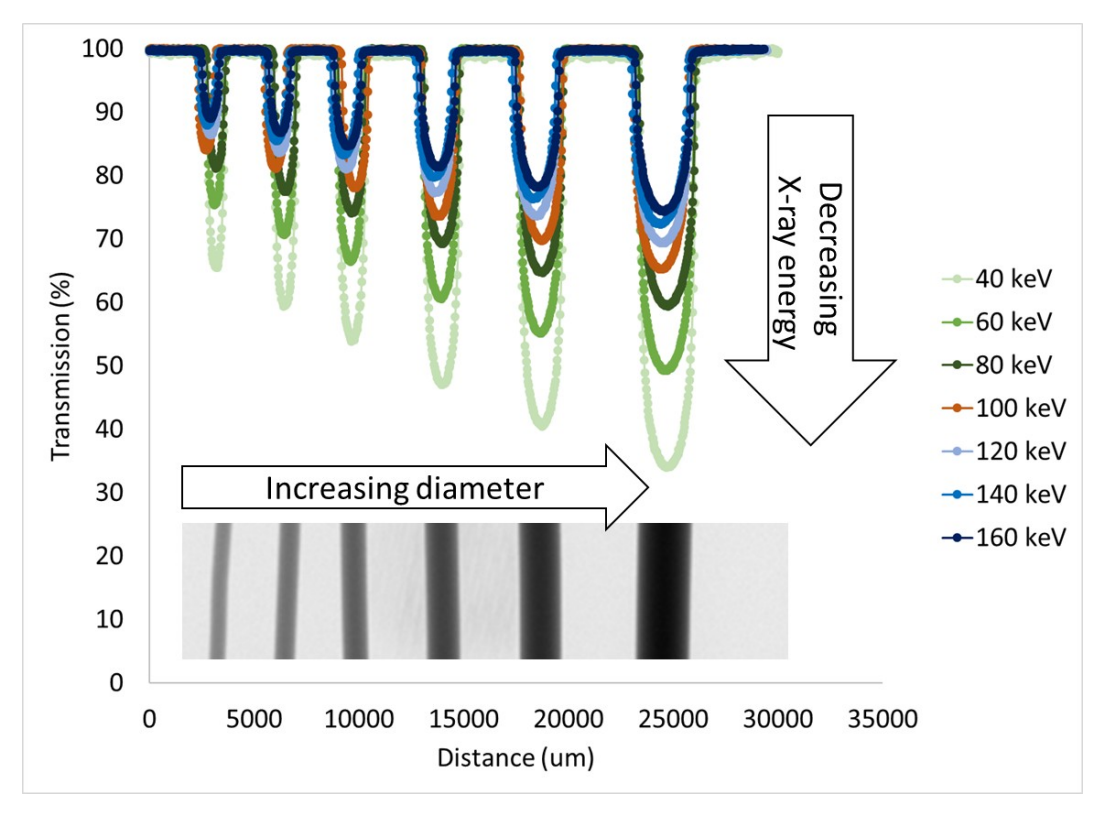


Figure 31. Aluminum rods of sizes ranging from 1 to 3 mm diameter and corresponding line profiles of the percent transmission at X-ray voltages ranging from 40 to 160 kV

Similar images and line profiles were collected on copper rods at the same voltages and diameter ranges to show the differences between different materials. Aluminum is a lower density metal of 2.7 g/cm<sup>3</sup> (g/cc), whereas copper has a much higher density of 8.96 g/cc, and therefore would have much lower transmission values. The minimums of the line profiles from Figure 31 were determined as well as the minimums from the copper line profiles in order to plot the transmission as a function of voltage and the results are shown in Figure 32. The aluminum (circles) and copper (triangles) have the same color for the same corresponding energy. The figure clearly demonstrates the fundamental principles that higher energies have increased transmission, thicker materials have less transmission, and higher density materials have less transmission. There is a significant difference between the aluminium and copper for the same sample diameter and energy. Even the smallest copper bar of only 1 mm diameter needs at least 80 keV energy for sufficient transmission through the sample of at least 10%. This illustrates the importance of sample size and minimum required voltage for scanning, particularly for higher density materials.

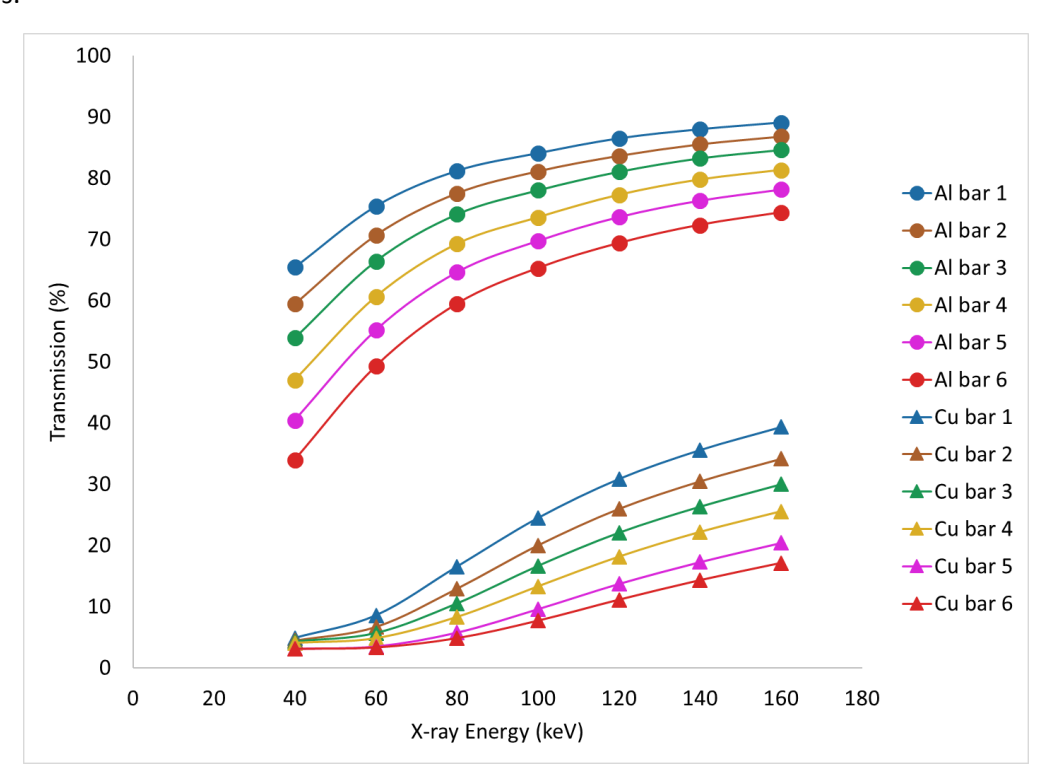


Figure 32. Transmission as a function of voltage for aluminum (circles) and copper (triangles) at increasing thicknesses from 1 to 3 mm for bars 1–6, respectively

#### 4.3 Noise

ASTM E 1441 describes noise as the variation in a measurement (or in an estimate or image derived from measurements) when it is repeated under nominally identical conditions [3]. Statistically random noise is distinguished from both systematic noise, which is not random and can come from a number of sources, and artifacts, which are essentially consistent biasing effects in XCT images. Random noise occurs in XCT images because there is both inherent statistical variation in the production of X-rays as well as statistical variation in the response of solid state detectors. When an image with random noise is digitally frame averaged n number of times, the magnitude of the noise fluctuation is decreased by the factor of the square root of n. In other words, the percent of original random noise remaining after n

frames is averaged is 100 \* (1/Vn) [5]. It is evident from the functionality of this equation that as the number of frames increases, the improvement in noise reduction becomes less and less effective. Thus, although frame averaging does not add a large amount of processing time applied to a few images like a few digital radiographs, there is a tradeoff between image improvement and total processing time if a relatively large number of images, such as is normally the case in XCT scans, will be averaged. A commonly used number of frames averaged is four, which reduces noise fluctuation by 50% and significantly reduces the noise level in a reasonable amount of processing time for large data sets.

In Nyquist-Shannon sampling theory, a given polychromatic (i.e., multiple frequency) temporal (or spatial) continuous function, f(x), with known maximum spatial frequency  $X_{max}$ , is determined by its sampled ordinates at a series of points spaced less than or equal to a distance of  $1/(2X_{max})$  apart [55]. The threshold  $2X_{max}$  is called the Nyquist rate and is an attribute of the continuous spatial input f(x) being sampled. The sample rate, R, must exceed the Nyquist rate for the samples to suffice to represent f(x). The threshold R/2 is called the Nyquist frequency and is an attribute of the sampling equipment. The number of projections, or view samples, used to reconstruct an XCT data set is one of the determining factors in image quality. Too large an interval between projections, or undersampling too few projections, results in the loss of accurate information about the physical geometry of the scanned object. Reconstructed images of an undersampled specimen would likely exhibit some type of regular angular variation in gray levels and associated loss of internal and edge physical information. A rule of thumb typically used in industry is to collect a number of projections equal to about 1.5 times the pixel width of the specimen's field of view, which essentially ensures that the scan space is adequately sampled over the course of recording projections. Sometimes it is desirable to oversample the scan space, especially when scanning at much higher resolutions when voxel sizes are small. This takes significantly more time, but provides finer physical geometric information for the reconstruction process and can help to mitigate the effects of high X-ray attenuation and related noise in the resultant XCT data.

Given that the X-ray technique and all other scanning parameters are sufficient to produce good quality reconstructed XCT data (images), significant undersampling will increase the noise floor to the point where it can severely negatively impact image quality. The increased noise level with a fewer number of projections is demonstrated in Figure 33 of a peanut butter cup candy. The images show the full field of view on the top row and digitally magnified images on the bottom row. With 1601 projections, the peanut butter filling is clearly seen in the center of the chocolate. There are both voids and a higher density (brighter) phase within the peanut butter filling that would be fairly easy to segment for quantitative analysis based upon the relatively high contrast and low noise. Reducing the number of projections to 801 still shows the voids and higher density phase, although there is slightly more noise (random gray level variation). Reducing the number of projections further to 401 significantly increases the noise level where it would be very challenging to successfully segment any particular phase. With only 201 projections, the results are so noisy that it is not only difficult to discern voids or higher density phases within the peanut butter, but it is also very difficult to clearly see the interface between the peanut butter and chocolate.

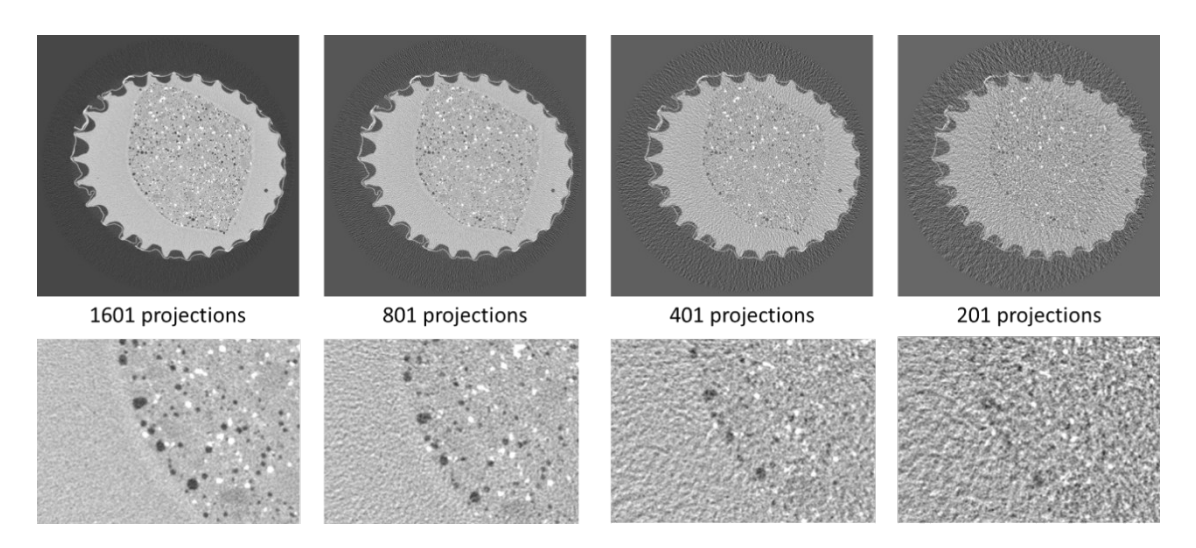


Figure 33. XCT scan of a peanut butter cup reconstructed with a fewer number of projections to demonstrate the influence on the noise level with the full field of view on the top and digitally magnified images at the peanut butter and chocolate interface on the bottom

## 4.4 Scanning Artifacts and Mitigation Strategies

As defined here, an artifact is anything in the reconstructed image that does not accurately reflect true physical structure in the object being inspected. Because they are not real, artifacts limit a user's ability to quantitatively extract density, dimensional, or other data from an image for primary or other more advanced calculations. However, as with any technique, the user can learn to recognize and be able to discount common artifacts subjectively, still allowing required data to be extracted from images [13]. An example of this is very high X-ray attenuation XCT scans, in which the object is a very high X-ray absorber for the energy being employed and very low, but sufficient, X-ray intensity is reaching the detector. If the detector response is high enough and overall scan parameters are sufficient, pertinent information can still be extracted from the image data even in the presence of recognizable artifacts.

There are several well-known scanning artifacts that are commonly observed in XCT scans. Some artifacts, such as beam hardening, typically occur in higher density samples. Others, like noise artifacts, can occur independently of the material being scanned if the number of projection images is inadequate. It is important to become familiar with scanning artifacts to discern what is real and part of the material microstructure versus an apparent microstructural feature that is not actually present. Many artifacts can be mitigated through changing the scan settings or correction factors during the reconstruction phase. Others are much more difficult or impossible to completely avoid, but still important to recognize to correctly interpret the results. This section summarizes several common scanning artifacts, describing what they are and, more importantly, how they can be avoided or substantially decreased. Artifacts included in this discussion include beam hardening, metal artifacts, ring artifacts, and motion artifacts.

#### 4.4.1 Beam Hardening

A vast majority of laboratory XCT systems utilize a polychromatic X-ray beam that emits a spectrum of X-ray energies over a range of intensities, which is called Bremsstrahlung radiation. Therefore, lower energy X-rays may be absorbed within the sample being scanned rather than transmitted through the sample to reach the detector. This effect happens progressively, meaning that as sample thickness increases, a proportionally higher number of low energy photons get absorbed. The absorption of the

lower energy X-rays leads to an average energy increase in the X-ray beam that reaches the detector, resulting in the well-known X-ray term "beam hardening". The beam hardening artifact most commonly appears in higher density materials due to the increase in absorption, whereas very low-density materials have very high levels of transmission and little absorption. With significant absorption, a cylindrical object as illustrated in Figure 34A (left) will have brighter edges and a darker center even though it is a homogenous material. The red dashed line illustrates the intensity profile across the cylindrical cross-section, and instead of a flat plateau across the homogenous material, a cupping-shaped dip in the intensity profile results due to more absorption at the edges of the sample over the course of the rotation.

Another type of beam hardening artifact is due to a scattering effect, which can be present in parts that have a more complex geometry. For the illustration of two cylinders in Figure 34B (right), there is more attenuation when the X-rays are traveling through both cylinders (along the dashed blue line) along a vertical path in the image than when the sample is rotated 90 degrees (horizontal path through image). This can result in an intensity profile with artificial peaks along the red dashed line that should not be present at all. The scattering beam hardening artifact is more common when the filtered back-projection reconstruction method is used [56].

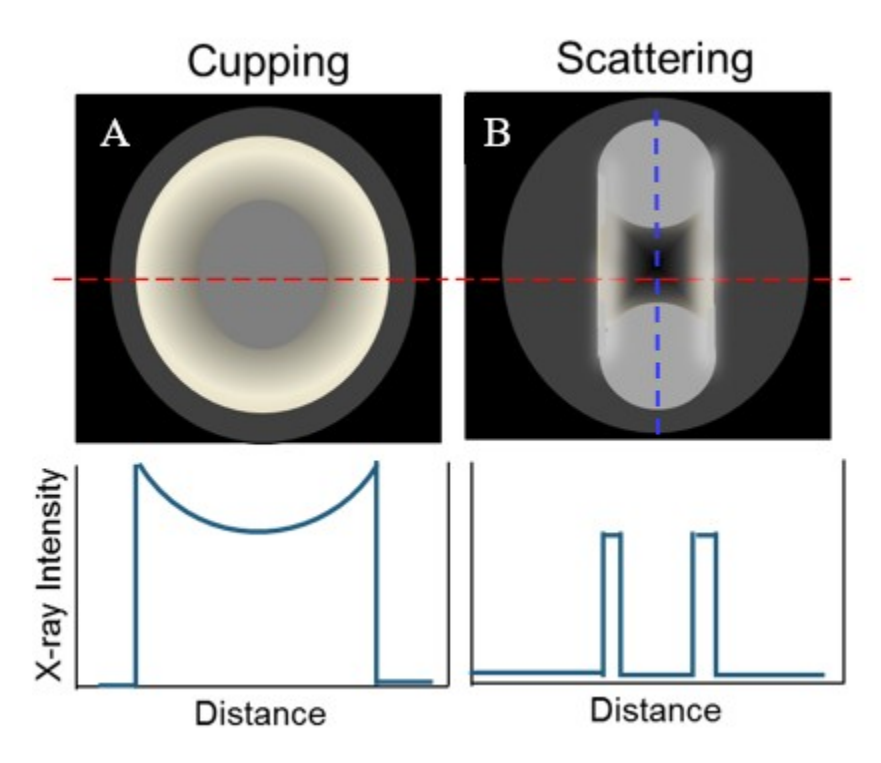


Figure 34. Illustration of beam hardening artifacts and X-ray intensity profiles along the red dashed lines: A) a cylindrical object resulting in a cupping-shaped intensity profile and B) two cylinders illustrating the scattering effect and erroneous intensity peaks

Beam hardening artifacts can be significantly reduced through the application of a filter. The filter absorbs lower energy X-rays within the filter material, allowing only higher energy X-rays to be transmitted through. This is called "hardening" the X-ray beam. Higher density material filters or thicker filters can absorb more X-rays, increasing the average energy of the X-ray beam and hardening the beam. This is illustrated in the schematic in Figure 35, which shows no filter and the low energy X-rays

being absorbed near the surface of the sample, medium energy X-rays being absorbed near the center of the sample, and only the high energy X-rays transmitting all the way through the sample to reach the detector, which would result in a significant cupping shape in the line profile. After adding a thin filter (Figure 35B), the low energy X-rays are absorbed within the filter material and a cupping shape would still result in the line profile, but to a lesser degree. With a thicker or higher density material filter (Figure 35C), the lower and medium energy X-rays are absorbed in the filter, leaving only the highest energy X-rays transmitting through the sample and reaching the detector. This would result in a plateaued line profile with minimal beam hardening artifacts. The drawback to this approach is that filters tend to reduce the overall photon count registered by the detector, so this may need to be offset either by increasing the beam current (which could increase spot size and therefore unsharpness) or frame integration time (which slows down scan time). Secondly, the SDD (or SID) may be decreased to recover intensity at the detector according to the inverse square law, but this approach may not be possible depending on the size and geometry of the object being scanned and/or "fitting" the object within the available cone beam envelope.

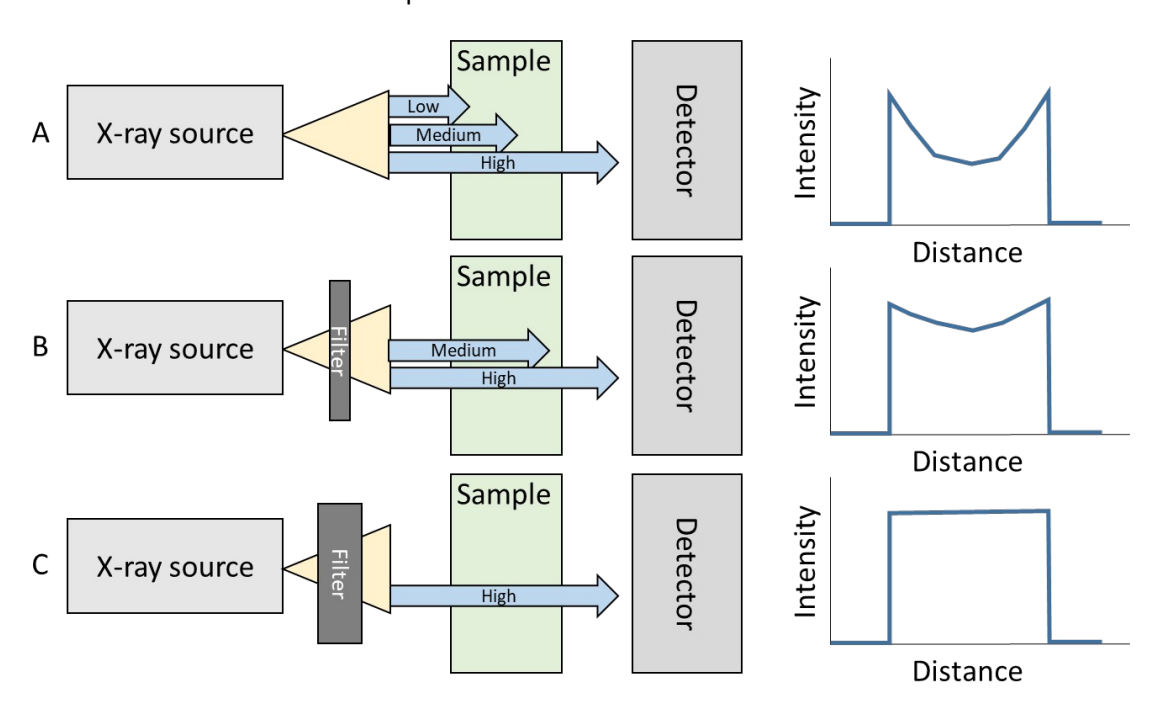


Figure 35. Schematic illustrating the influence of filters on beam hardening and resulting line profiles across a homogeneous material A) with no filter B) with a low density or thin filter and C) with a high density or thick filter

During the reconstruction phase, many (if not most) XCT systems have a beam hardening correction that can be applied to minimize the artifact. This is essentially a normalization function that balances out the overall intensity by superficially and preferentially boosting the signal toward the center of the image. Figure 36 (left) shows an example of line profiles drawn across an aluminum pin with varying levels of beam hardening correction. There is a significant improvement in the cupping-shaped line profile to be much flatter with an increase in the beam hardening correction. Figure 36 (right) shows the improvement in the plateau-shape of the line profiles with the application of increasing thicknesses of filters during the acquisition phase. With thicker filters, the signal intensity is lower and often needs to be compensated for by having longer exposure times per projection image, leading to longer scan times.

Additionally, there is increased noise in the line profiles of the thickest filters. A combination of filters during the acquisition phase and beam hardening corrections during the reconstruction phase are often used in conjunction with one another to achieve a consistent grayscale level throughout a homogenous material. In some rare situations it may be detrimental to use beam hardening corrections. For instance, if the part being scanned is composed of a functionally graded material, then applying these corrections may mask true variations in X-ray density through the thickness.

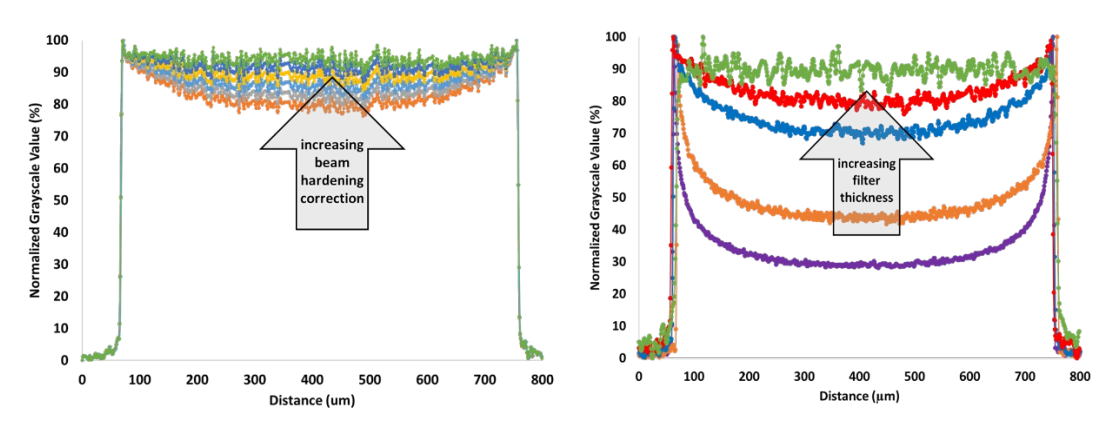


Figure 36. Normalized grayscale line profiles across an aluminum pin demonstrating A) the beam hardening correction applied during the reconstruction phase and B) the influence of increased filter thicknesses with no beam hardening correction applied

#### 4.4.2 Metal Artifacts

Metal artifacts are caused by small, high-density particles or pieces of material embedded in, or on the surface of, the sample itself. While these are not exclusive to metal particles, they are the most common culprit and most commonly seen when the bulk of the sample is non-metallic and there is a very small percent by volume of relatively high-density material contained within the scan volume. These features can be misleading and distracting as well as obscure parts of the sample in the surrounding vicinity. A common example of this is when the surface of the sample is not properly cleaned. This can also occur when tape is used for fixturing the sample and the tape itself may have some contamination on it. Composite laminates can also sometimes have some tiny fragments of metal embedded on the surface from cutting methods such as water-jetting. In electronics inspections, stray fragments of lead can often cause these issues. If such a small particle exists within the scan volume and is not somehow filtered out of the data upon reconstruction, it tends to leave an artifact behind. This can sometimes appear as a ring artifact or may have shadows cast around the feature combined with streaking as shown in Figure 37.

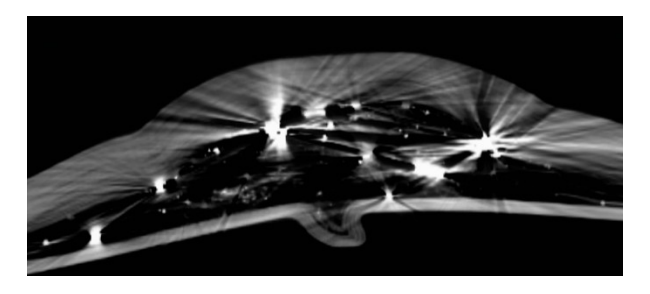


Figure 37. High-density metal particles (white) embedded within a low-density polymer composite leading to problematic metal artifacts

The other negative effect is that this may skew the resulting volume histogram because the software attempts to reconstruct with the higher density voxels treated as relevant data, but very disparate from the gray levels of interest that account for the rest of the volume. This gap between relevant and non-relevant data will tend to compress the relevant data into a lesser range of gray values, thereby reducing image latitude. Depending on the software used for the reconstruction or analysis, there may be filters available for reducing or eliminating such features, though when possible, it is best to try and remove these at the source. For example, in situations when there may be particles on the surface of the part, then additional cleaning steps such as ultrasonic cleaning prior to scanning may help reduce these. In some cases, it may also be possible to clip that feature out of the working volume and then reconstruct again.

### 4.4.3 Ring Artifacts

Ring artifacts are an inherent side effect of the reconstruction process. These are due to permanent or semi-permanent anomalies on the focal plane of the detector and may be caused by many possible reasons. When these anomalies are left in the raw images, that feature is swept through the reconstructed volume in a perfect circle that is centered around the rotation axis. A common cause is when there is a bad pixel in the detector that does not get adequately corrected using flatfield corrections. Sometimes these pixels are dead altogether, sometimes they are intermittent, and sometimes they are under-saturating (cool) or over-saturating (hot). Intermittent bad pixels can be tricky to resolve as they may be performing properly at the time the flatfield corrections are made, and only go "bad" during the scan. These tend to leave intermittent, dashed or partial rings behind in the reconstructed volume. If there is an entire column or bad or under/over-saturated pixels (as may be the case with some larger Complementary Metal Oxide Semiconductor [CMOS] detectors, which have multiple detector arrays tiled together), then these may create cylinder artifacts. The cylinder artifact is in essence a bunch of ring artifacts stacked on one another.

Another possible cause of ring artifacts is foreign debris on the surface of the detector screen (may be internal or external). Yet another possible cause may be debris on the exit aperture window of the X-ray source. This may be caused by overexcited target material such as tungsten that is projected onto the aperture window. Pitting of the target itself may cause similar looking artifacts or abberations, though those tend to be more blurred. Most of these features can be easily repaired by service or by image corrections. On the post-processing side, several XCT vendors offer some sort of ring artifact reduction routine as part of the software suite. This commonly employs tracked movements of the detector so the same detector pixel is not in the same location over the course of the scan. In some cases it may not be possible to remove ring artifacts altogether. This is sometimes the case toward the center rotation axis of the scan where the rings are more concentrated. In most scans, it is possible to locate the central scan axis simply by looking for a concentration of subtle ring artifacts toward the center of the volume, as illustrated in Figure 38. Strategic placement of the sample during scan setup can help to reduce the negative influence of these artifacts. For example, if there is a known region of interest in the part, it may be advisable to offset this region from the center of rotation to avoid these artifacts obscuring features of interest. In the case of hollow parts, it may be possible to avoid the center scan axis altogether.

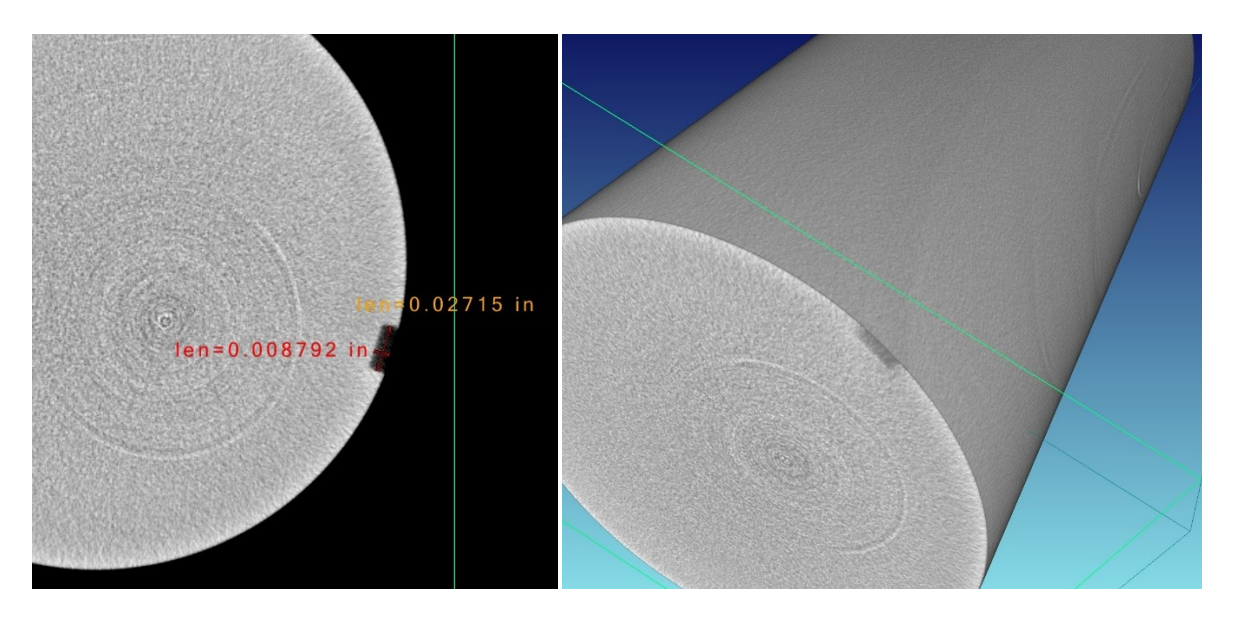


Figure 38. CT slice image (left) and 3D image showing cross-sectional slice (right) of a metallic bolt. This bolt was being used for a routine NDE inspection to assess notch and void detection sensitivity. Corrections to the images were not adequately performed and therefore pronounced ring artifacts were generated in the scan volume, consisting of sets of concentric cylinders which travel up the axis of the part (centered around the rotation axis).

#### 4.4.4 Motion Artifacts

Of all the artifacts in XCT reconstructions, motion artifacts may be the most difficult to eliminate, particularly for very small parts. This is because some degree of motion of the part, or fixture, is nearly impossible to eradicate altogether, and this motion gets amplified with increasing geometric magnification. Most reconstruction algorithms assume perfectly spaced step increments (i.e., projections) and zero movement of the part itself relative to the rotation stage. When a sample is large, rigid, has no "appendages" so to speak, and can ultimately be secured in a solid fashion, then issues typically do not occur. If, however, the sample is compliant, contains several moving parts, or if foam backing is being used to support the object (to provide an X-ray transparent support), then the part may settle during the scan. Cushioned foam tape can also be a particularly troublesome material for mounting parts because some tapes may have a tendency to relax. Also, some acrylic or silicone based adhesive tapes, often used to wrap parts, may creep.

To reduce these effects, there are a few strategies that may help. When using foam backing as an X-ray transparent support material, it helps to secure the part solidly enough that it is not loose, but not so tight that the structural pores in the foam itself are put under stress causing it to slowly compress. Another approach is to use more rigid and significantly less compressible low-density foams in a simplified structure to support and hold the part in place on the turntable. When using tape wraps to secure oddly shaped samples, it helps to provide two or more wraps, often in multiple directions (e.g., North/South over top of part, plus East/West or in a "hoop" direction around part). In all cases, when possible, it helps to let the sample rest a while in the final fixture/mount, and ideally inside the XCT system scan environment, for as long as possible, which also helps the sample adjust to the environmental temperature. This may not always be possible, but it helps to reduce motion blur since most of the displacement and settling occurs early. Other less common issues that may cause motion artifacts include objects hitting the sample or fixture during rotation (e.g., if some part of the sample/fixture apparatus is too close to the X-ray source or detector) or also if part of the fixture

releases during a scan (say a tape wrap coming loose). Similarly, in some cases the clamping fixture itself may slip on the rotation stage. This is more likely to happen during higher speed scans, or coarse scans, when the turntable is rotating at a higher velocity, effectively jerking the fixture at each step increment. This will often appear as an over-rotation of the part after completion. Another possible source of issues may be if there is some sort of hardware problem, such as a faulty rotation axis motor, sensor, or other hardware or synchronization issue.

Motion artifacts can sometimes be corrected during the reconstruction process, depending largely on the severity of the motion and the cause. Most XCT scanners collect data over the course of the scan that automatically accounts for the source stability and some account for the thermal stability of the X-ray tube in the correction algorithms. Reference images taken at the beginning and end of the scan can help correct for sample drifts as long as the motion is uniform. Large drifts or sample instability on the mount (such as a tilting motion) can generally not be corrected for and the sample would have to be rescanned. For high-resolution scans, sample thermal stability becomes more important and a "warm-up" scan can be conducted to bring the sample to a stable temperature within the XCT cabinet before starting the actual scan. Figure 39 illustrates severe motion artifacts in an ultra-high molecular weight polyethylene sample. The "wings" on the pores are a classic indicator of motion artifacts in a 180 degree scan.

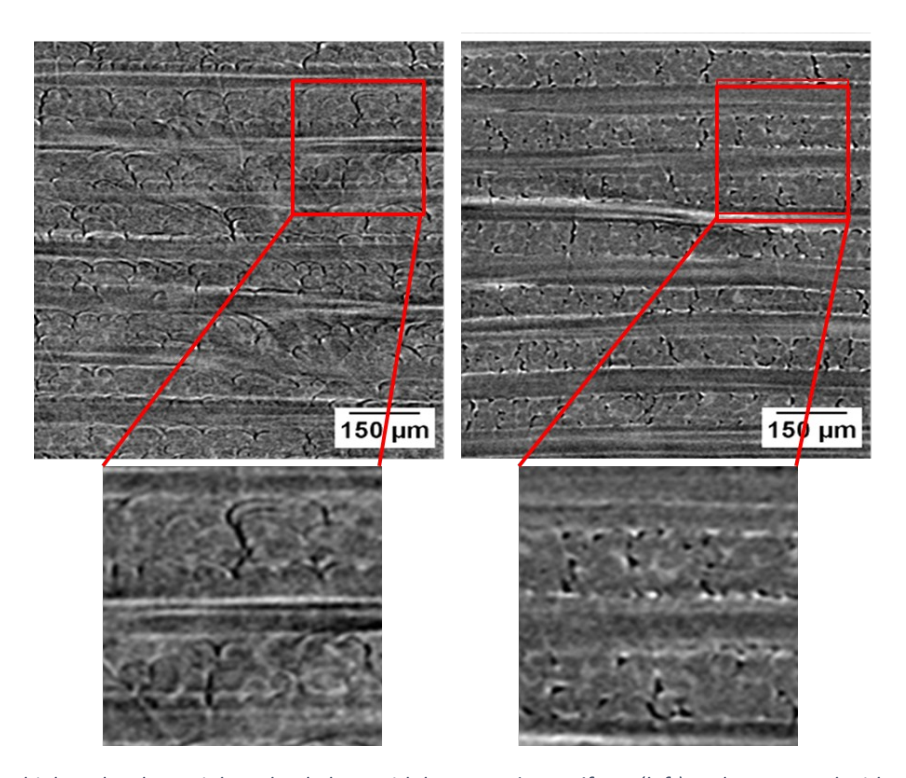


Figure 39. Ultra-high molecular weight polyethylene with large motion artifacts (left) and re-scanned with minimal sample motion

# 5. Conclusions

This chapter has provided an overview of XCT with applications and examples focused in the field of materials science. Section 1 introduced key definitions and concepts in the XCT fundamentals subsection and briefly discussed the history of the technological advancements. Other NDE methods were

described in order to discern the primary differences between XCT and other NDE techniques and their unique advantages. Complementary materials characterization methods were discussed, which can often be advantageous to obtain additional information that standalone XCT cannot provide.

Advanced scanning methods were summarized in Section 2. The use of a linear detector array can significantly reduce noise, especially for very high-density materials with complex shapes, and can sometimes be worth the additional scan time. Helical scanning is an excellent technique for very tall parts or when it is important to have direction alignment between the center of the X-ray source and the detector (such as horizontal crack detection). Dual energy scanning can increase contrast between phases of similar attenuations, drastically improving the likelihood of successful segmentation. Phase contrast enhancement methods can improve edge detection, especially for low-density materials. Diffraction contrast tomography can determine grain sizes and their orientations depending primarily on the crystal structure and size. Open XCT is a frameless scanning method that allows for geometry flexibility or the ability to scan specific regions of interest and a complex structure. Static XCT utilizes multiple sources and detector combinations to significantly reduce scan times and possibly capture dynamic events. Cryogenic or temperature controlled XCT can capture microstructures or microstructural changes that are only present at certain temperatures. It can also keep materials frozen, such as XCT imaging of snowflakes. In-situ mechanical tests can capture crack propagation and growth and other microstructural changes such as cavity formations. 4D scanning can capture motion either through a series of progressive static scans or dynamically if the event time and scan times are compatible. Lastly, an advanced reconstruction method discussed called iterative reconstruction and the reduction in image noise it produces was demonstrated.

Section 3 focused primarily on post-scan analyses. Advanced segmentation methods and automatic defect recognition were discussed. Tolerance deviation analysis was demonstrated to show the application for processing parameter improvements, quality control purposes, failure due to large thermal residual stresses, or comparisons on the same sample before and after testing. Porosity analysis demonstrated how the analysis could be applied for process parameter optimization and for further understanding the relationship with the mechanical properties. Void volumes, sphericity, and location dependence are all common quantitative analyses that can be performed on XCT datasets. Fiber orientation examples included the detection of misaligned fibers at a ply interface and the ability to measure chopped fiber orientations, which can be used to validate models or improve alignment with different processing conditions. Lastly, failure analysis examples were presented that included a circuit board failure, crack within an additively manufactured part, boroscope camera wire failure, and astronaut helmet blockage in the pitot tube. These failure analysis examples demonstrate that XCT can detect failures that are not possible through other NDE means or pinpoint locations of interest for further inspection.

Section 4 discussed several known limitations of XCT, including spatial resolution and X-ray transmission constraints, inherent random noise and methods to reduce problematic random noise, and common scanning artifacts as well as methods to reduce them. Many of the XCT resolution and transmission limitations can be overcome if there is the option to cut a sample down to a smaller size. Several scanning artifacts can be significantly mitigated or reduced to near imperceptible levels though either modified scanning techniques or correction factors during the reconstruction phase.

Overall, XCT has been shown to be a very powerful tool within the materials science and failure analysis communities. Recent advancements have allowed for significant improvements in resolution and therefore detectability. The technology of both the system hardware and the software (reconstruction and post-scan analysis) has rapidly advanced and is continuing to develop at a fast pace. The possibilities for new XCT applications and discoveries are very exciting.

#### Disclaimer

Many of the examples shown in this chapter were generated using Carl Zeiss Microscopy™ Zeiss Xradia 520 or North Star Imaging™ (NSI) X5000 XCT scanning systems, as they are the tools most available to the authors. It is important to note that other XCT manufacturers and systems have similar features and capabilities and the results presented in this text are not an endorsement for any one specific XCT manufacturer or their systems.

# 6. References

- 1. Radon, J., *Uber die bestimmung von funktionen durch ihre Integralwerte langs gewisser Mannigfaltigkeiten*. Journal of Mathematical Physics, 1917. **69**.
- 2. Dennis, M., *Industrial computed tomography. Nondestructive Evaluation and Quality Control*. ASM Handbook. Vol. 17. 1989.
- 3. ASTM International ASTM E1441-19, in Standard Guide for Computed Tomography (CT) 1995, ASTM International.
- 4. Pettersson, H., D.J. Allison, and N. Institute, *The Encyclopaedia of Medical Imaging*. The Encyclopaedia of Medical Imaging. 1998: NICER Institute.
- 5. Muelhauser, B. Optimizing image signal to noise ratio using frame averaging. 2015 [cited 2015.
- 6. Welvaert, M. and Y. Rosseel, *On the definition of signal-to-noise ratio and contrast-to-noise ratio for FMRI data.* PloS one, 2013. **8**(11): p. e77089-e77089.
- 7. Bryant, L. and E.M. Paul, *Nondestructive testing handbook : volume 3 : radiography and radiation testing*. American Society for Nondestructive Testing Penetrating Radiation Committee. 1985: American Society for Nondestructive Testing.
- 8. Oldendorf, W.H., The quest for an image of brain. Neurology, 1978. 28(6): p. 517.
- 9. Pietzsch, J. *Perspectives: With a little help from my friends*. Nobel Prize Outreach 26 Oct 2021]; Available from: <a href="https://www.nobelprize.org/prizes/medicine/1979/perspectives/">https://www.nobelprize.org/prizes/medicine/1979/perspectives/</a>.
- 10. Feldkamp, L.A., L.C. Davis, and J.W. Kress, *Practical cone-beam algorithm*. Journal of the Optical Society of America A, 1984. **1**(6): p. 612-619.
- 11. Elliott, J.C. and S.D. Dover, *X-ray microtomography*. Journal of Microscopy, 1982. **126**(2): p. 211-213.
- 12. Andrade, V.D., et al. nanoscale 3D imaging at the advanced photon source. 2016 [cited 2021.
- 13. CV Kropas-Hughes, S.N., Basics of Computed Tomography. Materials Evaluation, 2000. **58**(5).
- 14. ASTM E 1672-95a, in Standard Guide for Computed Tomography (CT) System Selection. 1995, American Society for Testing and Materials (ASTM).
- 15. Sundar, V., et al., Flaw Identification in Additively Manufactured Parts Using X-ray Computed Tomography and Destructive Serial Sectioning. Journal of Materials Engineering and Performance, 2021. **30**(7): p. 4958-4964.
- 16. Snow, Z., et al., Correction to: Flaw Identification in Additively Manufactured Parts Using X-ray Computed Tomography and Destructive Serial Sectioning. Journal of Materials Engineering and Performance, 2021. **30**(7): p. 4965-4965.

- 17. Silver, C.S.a.M. Comparison Between Single Slice CT and Volume CT. in Industrial Symposium on Computerized Tomography for Industrial Applications. 1994. Berlin.
- 18. Große Hokamp N, M.D., Shapira N, Chang DH, Noël PB, *Technical background of a novel detector-based approach to dual-energy computed tomography.* Diagnostic and Interventional Radiology, 2020. **26**(1): p. 68-71.
- 19. McCollough, C.H., et al., *Dual- and Multi-Energy CT: Principles, Technical Approaches, and Clinical Applications*. Radiology, 2015. **276**(3): p. 637-653.
- 20. Huda, W. and R.B. Abrahams, *Radiographic Techniques, Contrast, and Noise in X-Ray Imaging*. American Journal of Roentgenology, 2015. **204**(2): p. W126-W131.
- 21. Stock, S.R., *MicroComputed Tomography: Methodology and Applications*. 2009, Boca Raton: CRC Press.
- 22. Seltzer, J.H.a.S., *X-Ray Mass Attenuation Coefficients*, in *NIST Standard Reference Database 126*. 2004, National Institute for Standards and Technology: <a href="https://www.nist.gov/pml/x-ray-mass-attenuation-coefficients">https://www.nist.gov/pml/x-ray-mass-attenuation-coefficients</a>.
- 23. Mayo, S.C., A.W. Stevenson, and S.W. Wilkins, *In-Line Phase-Contrast X-ray Imaging and Tomography for Materials Science*. Materials (Basel, Switzerland), 2012. **5**(5): p. 937-965.
- 24. Guang-Hong, C., et al., *X-ray Phase Sensitive Imaging Methods: Basic Physical Principles and Potential Medical Applications*. Current Medical Imaging, 2010. **6**(2): p. 90-99.
- 25. Holzner, C., et al., *Diffraction Contrast Tomography in the Laboratory Applications and Future Directions.* Microscopy Today, 2016. **24**(4): p. 34-43.
- 26. McDonald, S.A., et al., *Non-destructive mapping of grain orientations in 3D by laboratory X-ray microscopy.* Scientific Reports, 2015. **5**(1): p. 14665.
- 27. Niverty, S., et al., A Forward Modeling Approach to High-Reliability Grain Mapping by Laboratory Diffraction Contrast Tomography (LabDCT). JOM, 2019. **71**(8): p. 2695-2704.
- 28. Shepard, L. New Bolton Center Pioneers Revolutionary Robotics-Controlled Equine Imaging System. 2015; Available from:

  <a href="https://www.vet.upenn.edu/about/press-room/press-releases/article/new-bolton-pioneers-equimagine">https://www.vet.upenn.edu/about/press-room/press-releases/article/new-bolton-pioneers-equimagine</a>.
- 29. *Robotic Manipulation To X-Ray Inspect Larger Parts*. 2021 [cited 2021; Available from: <a href="https://4nsi.com/robotic-manipulation-to-x-ray-inspect-larger-parts/">https://4nsi.com/robotic-manipulation-to-x-ray-inspect-larger-parts/</a>.
- 30. Burke, E.R., et al., *NDE of spacecraft materials using 3D Compton backscatter x-ray imaging.* AIP Conference Proceedings, 2016. **1706**(1): p. 110006.
- 31. Cramer, A., et al., Stationary Computed Tomography for Space and other Resource-constrained Environments. Scientific Reports, 2018. **8**(1): p. 14195.
- 32. Zellner, M.B., et al., *Considerations for the Design of a Multi-Color High-Speed X-Ray Computed Tomography Diagnostic*, A.R. Laboratory, Editor. 2014: Aberdeen Proving Ground.
- 33. Chandel, C., P.K. Srivastava, and P. Mahajan, *Micromechanical analysis of deformation of snow using X-ray tomography.* Cold Regions Science and Technology, 2014. **101**: p. 14-23.
- 34. JM Sietins, A.T., D VanOosten, J Robinette, *3-D Microstructural Interface Characterization with In-situ X-Ray Micro-Computed TomographyTensile Loading*, A.R.L. US Army Combat Capabilities Development Command, Editor. 2021.
- 35. Tilton, J.C., et al., *Best Merge Region-Growing Segmentation With Integrated Nonadjacent Region Object Aggregation.* IEEE Transactions on Geoscience and Remote Sensing, 2012. **50**(11): p. 4454-4467.
- 36. Gobert, C., et al., *Application of supervised machine learning for defect detection during metallic powder bed fusion additive manufacturing using high resolution imaging*. Additive Manufacturing, 2018. **21**: p. 517-528.

- 37. Kruth, J.P., et al., *Computed tomography for dimensional metrology.* CIRP Annals, 2011. **60**(2): p. 821-842.
- 38. Savio, E., *A methodology for the quantification of value-adding by manufacturing metrology.* CIRP Annals, 2012. **61**(1): p. 503-506.
- 39. Minetola, P., F. Calignano, and M. Galati, *Comparing geometric tolerance capabilities of additive manufacturing systems for polymers*. Additive Manufacturing, 2020. **32**: p. 101103.
- 40. Acevedo, R., et al., Residual stress analysis of additive manufacturing of metallic parts using ultrasonic waves: State of the art review. Journal of Materials Research and Technology, 2020. **9**(4): p. 9457-9477.
- 41. Hart, K.R., et al., *Increased fracture toughness of additively manufactured amorphous thermoplastics via thermal annealing.* Polymer, 2018. **144**: p. 192-204.
- 42. Rolland, H., et al., *Fatigue damage mechanisms of short fiber reinforced PA66 as observed by insitu synchrotron X-ray microtomography.* Composites Part B: Engineering, 2018. **143**: p. 217-229.
- 43. Bie, B.X., et al., *Orientation-dependent tensile deformation and damage of a T700 carbon fiber/epoxy composite: A synchrotron-based study.* Carbon, 2017. **121**: p. 127-133.
- 44. Maksimcuka, J., et al., *X-ray Tomographic Imaging of Tensile Deformation Modes of Electrospun Biodegradable Polyester Fibers.* Frontiers in Materials, 2017. **4**(43).
- 45. Wright, P., et al., *Ultra High Resolution Computed Tomography of Damage in Notched Carbon Fiber—Epoxy Composites*. Journal of Composite Materials, 2008. **42**(19): p. 1993-2002.
- Wirjadi, O., et al., Characterization of multilayer structures in fiber reinforced polymer employing synchrotron and laboratory X-ray CT. International Journal of Materials Research, 2014. **105**(7): p. 645-654.
- 47. Goris, S. and T.A. Osswald. *Fiber orientation measurements using a novel image processing algorithm for micro-computed tomography scans*. 2015.
- 48. Dierig, T., et al. Fiber composite material analysis in aerospace using CT data.
- 49. Westenberger, P., P. Estrade, and D. Lichau. Fiber orientation visualization with Avizo Fire®.
- 50. Blanc, R. and P. Westenberger. Comparison of fiber orientation analysis methods in Avizo.
- 51. Emerson, M.J., et al., *Individual fibre segmentation from 3D X-ray computed tomography for characterising the fibre orientation in unidirectional composite materials.* Composites Part A: Applied Science and Manufacturing, 2017. **97**: p. 83-92.
- 52. Czabaj, M.W., M.L. Riccio, and W.W. Whitacre, *Numerical reconstruction of graphite/epoxy composite microstructure based on sub-micron resolution X-ray computed tomography.*Composites Science and Technology, 2014. **105**: p. 174-182.
- 53. Sietins, J.M., J.C. Sun, and D.B.K. Jr, *Fiber orientation quantification utilizing X-ray micro-computed tomography*. Journal of Composite Materials, 2020. **55**(8): p. 1109-1118.
- 54. Patterson, B.M., et al., *Dimensional Quantification of Embedded Voids or Objects in Three Dimensions Using X-Ray Tomography.* Microscopy and Microanalysis, 2012. **18**(2): p. 390-398.
- 55. Shannon, C., *Communication in the presence of noise.* Proceedings of the Institute of Radio Engineers, 1949. **37**(1): p. 10-21.
- 56. Boas, F.E.a.F., Dominik *CT artifacts: causes and reduction techniques.* 2012. **4**(2): p. 229-240.

# 7. Acknowledgements

The authors would like to thank the numerous collaborators who have samples presented within this chapter for their permissions to include the examples within this reference book. Additionally, the authors would like to thank Dr. Timothy Walter at DEVCOM ARL for his insightful discussions and

assistance. Lastly, the authors would like to thank external collaborators including industry partners and XCT manufacturers for their training and insightful discussions over the years, especially Carl Zeiss Microscopy $^{\text{\tiny M}}$ , NorthStar Imaging $^{\text{\tiny M}}$ , and Bruker Skyscan $^{\text{\tiny M}}$ .

#### **DEVCOM ARL:**

Dr. Brandon McWilliams

Dr. Tom Plaisted

Dr. Andy Gaynor

Ms. Jessica Sun

Dr. Dan Knorr

Dr. Andy Bujanda

Dr. Anindya Ghoshal

Dr. Michael Walock

Mr. Marc Pepi

Dr. Lionel Vargas-Gonzalez

#### NASA GSFC:

Materials Engineering Branch/541

Dr. James Tilton

Dr. James Garvin

Mr. Bruno Munoz

Mr. Antonio Moreno

Mr. Chris Hoffman

Mr. Stephen Lebair

Mr. Nathan Smith

Dr. Keith Gendreau

Dr. William Prosser

Mr. Eric Burke

#### **Biography and Photo**

**Jennifer Sietins** 



Dr. Jennifer Sietins is a Materials Engineer at the U.S. Army Combat Capabilities Development Command Army Research Laboratory (DEVCOM ARL). She completed her BS and MS degrees in Materials Science and Engineering (MSE) at Virginia Tech in 2007 and 2008. She graduated with her Ph.D. in MSE from the University of Delaware in early 2014, before starting at DEVCOM ARL as a post-doc and transitioning to

federal employment. Her primary research interests have focused on the development of fundamental material relationships through XCT for a wide variety of material classes. She particularly enjoys establishing new analysis techniques to quantify the XCT observations. Her work has helped identify failure mechanisms, optimize manufacturing processes, and make new discoveries about material microstructures.

Justin S. Jones



Dr. Justin S. Jones is the NDE Subject Matter Expert and a senior Materials Engineer for the NASA Goddard Space Flight Center in Greenbelt, Maryland. An alumnus of the Johns Hopkins University, Dr. Jones has worked at NASA GSFC since 2010 and has been active in the field of NDE for over 22 years. Aside from regular duties as GSFC's NDE lead, Dr. Jones has recently focused efforts on the NDE of additively manufactured parts, NDE in support of geology for planetary exploration, and advocating the use of NDE inspection tools for in-space applications. Dr. Jones is experienced with several NDE methods, with special focus in recent years on X-ray CT technology, standards development, and capability advancement.